AN EXPERIMENTAL STUDY ON REPAIR OF STEEL BRIDGE PILES USING GFRP CONCRETE-FILLED JACKET

A Thesis

Presented to the Faculty of the

Department of Civil and Environmental Engineering

University of Houston

In Partial Fulfillment of the

Requirements for the Degree Master of Science in

Civil Engineering

by

Ali KAYA

December 2014

AN EXPERIMENTAL STUDY ON REPAIR OF STEEL BRIDGE PILES USING GFRP CONCRETE-FILLED JACKET

Ali KAYA

Approved:

Chair of the Committee
Bora Gencturk, Assistant Professor,
Civil and Environmental Engineering

Committee Members:

Co-Chair of the Committee
Mina Dawood, Assistant Professor,
Civil and Environmental Engineering

Ali K. Kamrani, Associate Professor,
Industrial Engineering

Suresh K. Khator, Associate Dean,
Cullen College of Engineering

Roberto Ballarini, Professor,
Department Chair

ACKNOWLEDGEMENTS

I wish to express my genuine gratitude to my advisor and mentor, Dr. Bora Gencturk, for his enthusiastic encouragement and patient guidance during this research. Also, I would like to thank my co-advisor, Dr. Mina Dawood for his suggestions, encouragements, and useful critiques during the course of this research. It was a great opportunity and honor to benefit from their wealth of knowledge and extensive personal experience. I have been extremely lucky to have a supervisor and a co-advisor to overcome many problems and finish this study. Also, I would like to kindly acknowledge the generous financial support provided by Turkish Republic, Ministry of National Education. I also would like to thank Dr. Ali K. Kamrani for being one of my committee members and providing valuable feedback on my research.

I would like to kindly acknowledge the donation of the glass fiber reinforced polymer materials by QuakeWrap without which this research could not have realized. I gratefully acknowledge my friend and graduate student Hossein Karagah in helping me carry out experimental work in the laboratory. Also, I wish to thank my other colleagues in the Department for being continually supportive.

Lastly, to my caring, loving, and supportive wife, Betul: my deepest gratitude. Her support, encouragement, quiet patience and unwavering love were undeniably the bedrock upon which the past two years of my life have been built. Her tolerance of my occasional grumpy moods is a testament in itself of her unyielding devotion and love. I thank my parents, Nevzat and Lutfiye, for their faith in me and allowing me to be as ambitious as I wanted. Also, my sisters Havva, Rumeysa, and Melike receive my deepest gratitude and love for their dedication and their support.

AN EXPERIMENTAL STUDY ON REPAIR OF STEEL BRIDGE PILES USING GFRP CONCRETE-FILLED JACKET

An Abstract

of a

Thesis

Presented to

The Faculty of the Department of Civil and Environmental Engineering

University of Houston

In Partial Fulfillment of the

Requirements for the Degree Master of Science in

Civil Engineering

by

Ali KAYA

December 2014

ABSTRACT

Many bridges and structures in the United States that are supported on steel piles exhibit inadequate strength due to increasing load demand and aging due to corrosion The combination of increased load demand and reduction of capacity due to corrosion-induced section loss can lead to unexpected buckling of the piles. Several techniques are available to repair these structures to meet the increasing demand and enhance their safety. This thesis investigates the effectiveness of a glass fiber reinforced polymer (GFRP)-based system for rapid repair of buckled steel piles. The system consists of a GFRP tube, which is formed on-site and subsequently filled with an expansive concrete. Thirteen-buckled steel H-piles with varying degrees of section loss to simulate corrosion were repaired and tested to failure under axial loading. The research results show that the repair system can restore the capacity of the piles comparable to the undamaged conditions.

TABLE OF CONTENTS

LIST OF FIGURES

LIST OF TABLES

1 Introduction

1.1 Overview of Research

In the last a few decades, various bridges and ports supported on steel piles have been identified in the United States to have inadequate load carrying capacity due to corrosion, increasing traffic capacity, and aging (usually associated with corrosion). These structures have to be re-built or strengthened. There are various strengthening techniques such as welding or bolting steel plates, and using composite materials. Researchers have investigated the use of new composite materials with regard to cost, time, and ease of application. The mechanics of fiber reinforced polymer (FRP) composite materials are very different from the mechanics of traditional building materials such as steel. Over the past 20 years FRP laminates have been studied and used increasingly for civil engineering applications such as the strengthening and repair of concrete, steel, timber, and masonry members.

With further development of composite materials throughout the world, fiber reinforced polymer (FRP) has become a useful tool for repairing and strengthening steel structures, particularly steel bridge girders and railroad bridge piles. In recent years, “I” shaped steel members, which were used in numerous bridges, have a common problem of corrosion because of their exposure to environmental factors. These steel structures show various levels of deterioration in the flanges and webs of piles, and braces, which results in a loss of capacity and they have to be repaired or replaced. Most of time, replacement is more expensive than repair and strengthening. In the United States, FRP has become a

useful repair approach due to its high strength to weight ratio, durability, and ease of application (Karimi et al., 2012).

In the recent years, many companies and researchers have developed glass fiber reinforced polymer (GFRP) and carbon fiber reinforced polymer (CFRP) sheets. These FRP products are lightweight, corrosion resistant, highly versatile, and have a high strength.

While FRP jacketing of concrete piles is a well-established technique, there has been substantially less research conducted to investigate the effectiveness of this method to retrofit steel compression members as compared to flexural strengthening of concrete columns. GFRP may be preferable in cost-sensitive applications where the higher strength and stiffness of carbon fibers are not required to provide satisfactory structural performance. Replacing corroded or damaged steel piles or columns typically requires major replacement of substantial portions of the rest of the structure which may not otherwise require replacement. As reviewed below, researchers have investigated the use of GFRP laminates to strengthen and repair steel piles. The GFRP jacket provides a confining stress while the concrete is expanding. Researchers also have worked on strength, modulus of elasticity, and density of FRP required for strengthening applications. FRP jacketing minimizes the environmental effects and therefore the rate of environmental degradation of the pile is reduced. Additionally, the strength and ductility of the system is increased due to FRP confinement. The axial capacity of confined concrete is higher than that of an unconfined member; the stress-strain curve on the level of confinement is shown in Figure 1.1. However, the shape of the cross section influences the effectiveness of the confinement. Confining circular columns is more effective than

confining rectangular piles with FRP jackets. Therefore, in strengthening steel piles using FRP jackets, a circular section is preferred.

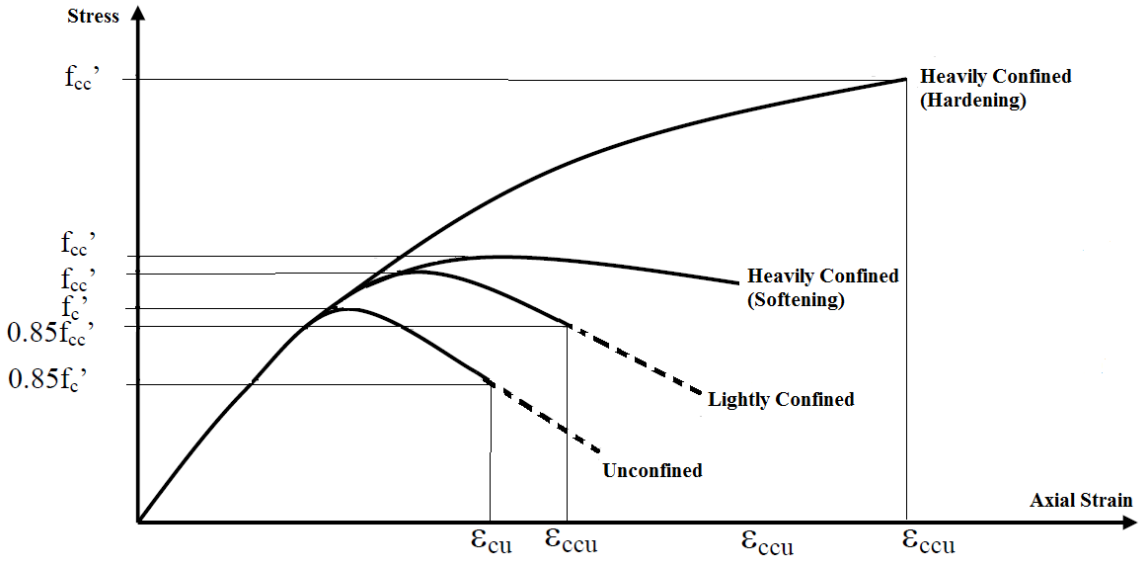

Figure 1.1. Stress- Strain Curve of Concrete with Different Levels of Confinement

1.2 Objective of Research

The objectives of this study are:

1) To evaluate the feasibility of a GFRP jacket to repair corroded and buckled steel H-piles.
2) To investigate experimentally the structural behavior of buckled steel piles that are repaired with concrete-filled GFRP tubes in terms of modes of failure and structural properties (i.e., stiffness, strength and ductility).

1.3 Outline of Thesis

This thesis is divided into five chapters. After this first introductory chapter, chapter 2 presents a literature review of previous studies on strengthening of structural members using FRP. Chapter 3 describes the monotonic compression experiments

conducted on thirteen buckled steel H-piles that were tested previously and repaired here. Chapter 4 presents and discusses the results of the experimental program and includes material test results on GFRP, steel and concrete. Chapter 5 presents conclusions and recommendations for future research.

2 Literature Review

2.1 Review of Previous Work

This chapter is a review of previous similar experimental investigations on strengthening of structural members with GFRP or CFRP.

In the last decades, several researchers have studied the use of concrete-filled FRP tubes as a technique to increase the buckling capacity of steel compression members. Generally, this technique includes two steps: wrapping the damaged steel pile due to corrosion or axial loading using FRP laminates and filling the jacket with concrete. Figure 2.1 shows a schematic of this technique to increase the buckling capacity of steel compression members.

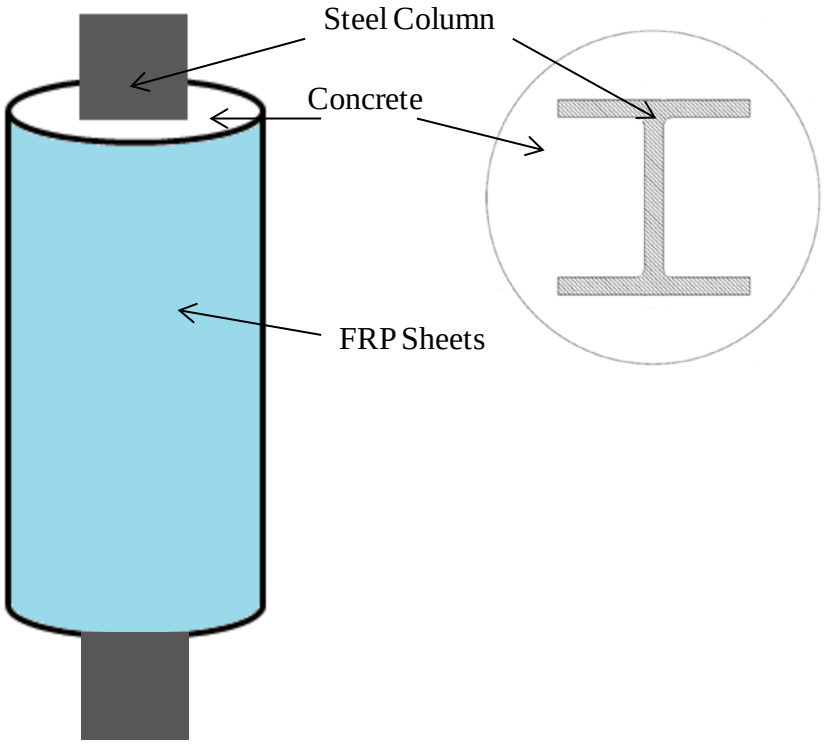

Figure 2.1. Illustration of the Proposed Strengthening Approach for Steel Piles

The FRP jacketing method was successfully applied for strengthening of steel columns by Liu et al. (2005). Various retrofit lengths were investigated to study the effect of the length of the repair on the capacity and overall response of seven repaired steel columns that were 10 ft long with an S4x9.5 cross-section. Two of the columns were used as a control specimen. One of the control specimens was notched in the center zone to simulate a state of severe corrosion and the second one was virgin. The flanges of the columns were machined to represent the section loss due to corrosion. The columns, with simulated corrosion, were subsequently repaired with concrete-filled GFRP tubes and tested monotonically to failure. The inside diameter of the GFRP tube was 6.4 inches. The thickness of the GFRP was 0.1 inch. Five test units were retrofitted between 3 and 5 ft lengths. It was noted that as the retrofit length increased, the ultimate load carrying capacity increased and the columns failed due to inelastic flexural buckling (Liu et al., 2005). Expansive concrete was found to increase the axial load carrying capacity more than the non-expansive concrete for providing positive pressure which was believed to enhance the bond between the steel and the concrete and improve the overall performance of the system. Liu et al. (2005) did not strengthen the entire length of the steel column to reduce the amount of materials used and due to practical difficulties in strengthening the entire length. Discrepancies were observed between the theoretically calculated and experimentally observed buckling loads and these discrepancies were attributed to the eccentricity of the axial load, the inaccuracy in the assumed deflected shape of the column, and the presence of cracks in concrete.

In a similar study, steel columns were retrofitted with GFRP for their entire height (Karimi et al., 2010). Two types of FRP tubes, a concrete filled tube with and without a

chemical admixture to reduce the shrinkage of the concrete were tried. Seven columns were tested in this program. Three of the columns were tested as a control specimen. The I-section steel columns were 20 inches long with a W150 x 14 cross-sections which is classified as a compact section according to CAN/CSA S16-09 (CSA 2009). The inside diameter of the GFRP tubes was 8.3 inches and the outside diameter of the tubes was approximately 8.6 inches. The thicknesses of the two types of GFRP were 0.13 and 0.14 inch. The two GFRP types had different mechanical properties such as lateral tensile strength, lateral tensile modulus, compressive strength and tensile strength. Columns were tested using displacement controlled loading at a rate of 0.1 mm/min. Strain gauges were used to measure the axial and hoop strains at the mid-height of the columns. Research showed that shrinkage reduced the benefits of the confinement of concrete and resulted in a lower compressive strength. Axial stresses in the confining jacket were affected from the gap and the confinement was reduced or delayed. Installation of the proposed system increased the compressive strength of the concrete in the composite specimen by between 40 and 80%. The axial strength and ultimate axial strain were increased by 25 and 20%, respectively.

Feng et al. (2013) proposed a strengthening method for steel columns using a mortar-filled GFRP tube, which was wrapped with FRP fabrics at the ends. The objective was to improve the buckling resistance of steel members, which were made of Q345 (Chinese Standard GB/T 228-2002) steel having four different cross shaped sections: I section, cross shaped section, round tube and square tube. The investigated parameters included the cross section of the steel members, slenderness, and number of FRP fabric layers. Eighteen specimens were used in this experimental program. Seven of the

columns had cross-shaped sections, seven had I-sections, two were round tubes, and two were square tubes. The columns had various lengths between 30.7 and 114 inches. The inside diameter of the GFRP tube was 3.5 inches with a thickness of 0.26 inch. In this study, test matrix included five scenarios. Two of the scenarios had the same nominal slenderness ratio and different FRP fabric layers at the ends of GFRP tubes. The specimens in other two scenarios had different slenderness ratios. The last scenario had the same slenderness and FRP fabric layers, but different cross-sectional shapes. After strengthening the steel using mortar-filled FRP tubes, it was observed that the load bearing capacity increased by 215%. In addition, the ductility was increased by 877%. Longitudinal splitting failure was prevented by two FRP fabric layers at the end of the FRP tube. It was found that more than two FRP fabric layers at the end of the GFRP tube did not significantly affect the load bearing capacity and ductility. The specimens with greater slenderness failed by global buckling instead of local buckling.

The effect of the slenderness of confined columns on the compressive strength, elastic axial stiffness, and energy dissipation capacity was investigated by Karimi et al. (2012). The strengthening of an I-shaped steel column was accomplished by pouring concrete between the flanges then wrapping it with one layer of GFRP. After the GFRP wrapping, two additional layers of CFRP sheets were wrapped around the specimen. Nine columns with W150 x 14 (Canadian Institute of Steel Construction, 2011) cross-sections were tested in this experimental program. Three of the tested specimens were bare steel columns that were 20, 60, and 118 inches long. Confined columns were between 20 and 118 inches long. Eight inches overlap was used in this study to avoid premature failure due to debonding. The resulting specimens were square composite columns. The results

showed that the height of the specimens was important in the failure of the composite specimens because specimens were losing stability before the activation of the confinement. The confinement of FRP did not affect the elastic axial stiffness (i.e., below 0.002 strains). The energy dissipation capacity of the strengthened columns was increased by 2-14 times compared to the unstrengthened columns. It was confirmed that when the slenderness was larger than 1.0, the confinement did not work properly due to overall buckling failure before the confinement was engaged. With increasing column height, the ductility decreased. The ratio of the elastic axial stiffness and ultimate axial strain were 2.1 to 2.5 and 1.0 to 2.6, respectively. Shortest control specimen failed by local buckling of the steel flanges and web, but others failed by bending (global buckling) of the specimens.

Inhibiting steel brace buckling with CFRP was investigated by El-Tawil et al. (2009). This technique included two steps: (1) attaching two mortar blocks to the braces, (2) wrapping the entire system with CFRP sheets. Seven single and double angle braces were tested in this experimental program with reversed axial loading. The used angle section was L2.5 x 2.5 x 3/16. The double angle specimens were prepared by welding together at three points. In this experimental program, the slenderness ratio was 110 for double angle specimens and 175 for single angle. Pinned end and semi fixed conditions were tested. For double angle specimens, there were two control specimens which were pinned and semi fixed. Two single angle specimens were tested; one of them was control specimen. Four and six layers of CFRP were tested. As expected all control specimens buckled elastically in compression at early stages of testing. However, confined specimens had significant increase in the load carrying capacity. Using CFRP wrap,

energy dissipation capacity increased by 270% compared to the unwrapped specimens. Double angle specimens benefited more from the strengthening than single angle counterparts.

Strengthening of circular steel columns with CFRP was also investigated (Han et al., 2010). Tubular columns were strengthened and tested under constant axial load and cyclic flexural load with increasing amplitude to investigate the strength, ductility, stiffness, and energy dissipation characteristics. The level of axial load and the number of FRP layers were changed as test parameters. A total of eight specimens were tested. Four of the specimens had a square cross-section and the others had a circular cross-section. The outside dimensions of specimens were 5.9 inches and the overall length of a specimen was 59 inches. The diameter and the thickness of the strengthened steel tube were 3 and 0.09 inches, respectively. One and two CFRP layers were used. A similar failure mode was observed for all specimens. At the peak load, the rupture of longitudinal CFRP jacket occurred with increasing mid- span displacement. Lateral load capacity dropped suddenly after the rupture followed by circumferential rupture. As a result, the number of CFRP layers affected the elastic stiffness only slightly, while the elastic plastic stiffness of the specimen increased with increasing number of layers. The strength increase of circular and square columns wrapped with one layer FRP were 20.2 and 12.2%, respectively. For square specimens, the residual strength was similar for one and two layers of CFRP. However, residual strength was different between one and two layers for circular specimens. Specimens showed energy dissipation before the rupture of longitudinal CFRP. Increasing the number of CFRP layers improved the ultimate strength

of the specimens. Number of layers moderate affected the ductility and energy dissipation.

2.2 Research Significance

Several techniques are available to repair steel piles to meet the increasing demand and enhance their safety. This thesis investigates the effectiveness of a glass fiber reinforced polymer (GFRP)-based system for rapid retrofit of buckled steel piles. Thirteen steel piles with different degradation on flanges and web repaired with GFRP. This repairing system consists of a GFRP tube, which is formed on-site and subsequently filled with an expansive concrete. The behavior of concrete columns strengthened with GFRP or CFRP tube has been researched extensively. However, relatively little research was conducted to investigate effectiveness of a GFRP-based or CFRP-based system for rapid repair of steel piles.

3 Experimental Program

This chapter presents the details of the experimental program including the test setup, test matrix, instrumentation, and the loading protocols. As mentioned earlier, 13 reduced-scale steel H-piles with W4x13 cross-section were repaired and tested. The details of previous research where the piles were reduced in their cross-section to simulate corrosion and tested under axial loading are also included in this chapter.

3.1 Previous Research

The short steel piles that were repaired with GFRP in this research were obtained from a previously conducted experimental program (Karagah and Dawood, 2013). A total of 13 short steel piles were milled to simulate the loss of cross-section caused by corrosion. Degradation of the flange thickness was between 0 and 75% while the degradation of the web thickness was between 0 and 100%. In addition, several of piles were machined to simulate the asymmetrical corrosion of the flanges, while others included a void in the web (complete through-thickness corrosion of the web), or reduction of the flange width in addition to reduction of the flange and web thicknesses. The simulated corrosion patterns are shown schematically in Figure 3.1.

Each of the specimens was designated with a label made up of five parts. The first part of the label shows the reduction in the thickness of the flange. The second part shows the reduction in the thickness of the web. The third part indicates whether there is a void in the web or not, as a “NV” or “V”. The fourth part shows symmetric or unsymmetrical corrosion of the flanges, as “S” or “US”. If there is a reduction in the width of the flanges, the fifth part shows this as “WR”. As an example “75/60/NV/US/WR” means that the steel pile has 75% reduction of the flange thickness, 60% reduction of the web

thickness, no void, unsymmetrical degradation of the flange, and reduction of the flange width. Figure 3.1 schematically shows the symmetric and asymmetric reduction of the steel piles at various elevations, including the web voids, and flange width reduction.

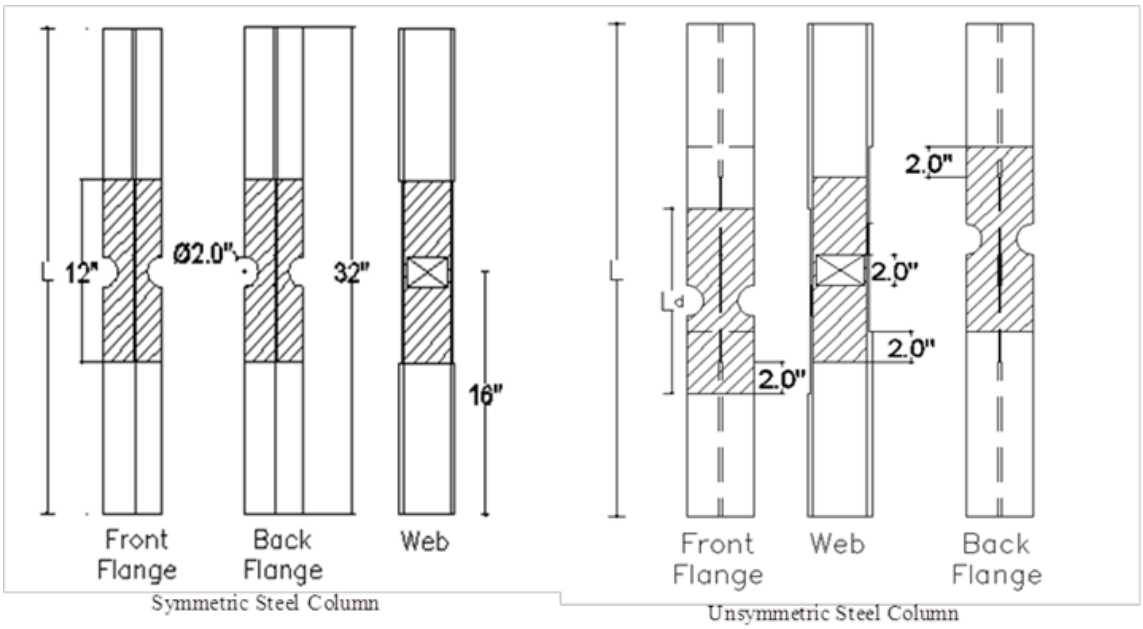

Figure 3.1. Symmetric and Unsymmetric Damage in Steel Piles

Table 3.1 provides the details of the short steel piles. Twelve piles had reduced thicknesses of flange and web and were tested to determine the effects of corrosion on axial load capacity. One of the steel piles did not have any degradation and it was used as a control specimen. Specimens had flange thickness reductions of 0, 50 to 75% and 30 and 60% web thickness reduction. Four of the piles had a two inch void in the web. Four of the piles had unsymmetrical flange reduction. Three of the piles had reductions in the flange. All of the piles, prior the strengthening, failed by inelastic buckling. Failure modes included global buckling, flange local buckling, and flange local buckling followed by web local buckling. Failure modes of specimens before repair are shown in

Figure 3.2. In this research the corroded and damaged piles were repaired with concrete-filled GFRP jackets and retested.

Table 3.1. Details of the Short Steel Piles Tested Previously (Karagah et al., 2013)

	Designation		Axial Strength (kips)	Void in Web	Flange Width Reduction	Unsymmetric	Reduction of Flange Thickness (%)	Reduction of Web Thickness (%)	$b_{f,min}$ [a] (in)	$t_{f,min}$ [b] (in)	$t_{w,min}$ [c] (in)	A_{min} [d] (in^2)
	Karagah et al. (2013)	This Study										
Group #1	0/0	G1/2/NR-1	215	No	No	No	0	0	4.167	0.36	0.303	4.11
	0/30	G1/2/NR-2	201	No	No	No	0	30	4.17	0.353	0.213	3.74
	0/60	G1/2/NR	178	No	No	No	0	60	4.168	0.357	0.121	3.45
Group #2	50/0	G2/3/NR-1	117	No	No	No	50	0	4.169	0.155	0.285	2.47
	50/30	G2/3/NR-2	130	No	No	No	50	30	4.162	0.183	0.206	2.32
Group #3	75/0	G3/2/4#3-1	92	No	No	No	75	0	4.173	0.072	0.284	1.69
	75/60	G3/2/4#3-2	70	No	No	No	75	60	4.173	0.106	0.106	1.33
	75/60/NV/US	G3/3/4#3	57	No	No	Yes	75	60	4.174	0.079	0.099	1.01
	75/60/NV/US/WR	G3/2/4#4	70	No	Yes	Yes	75	60	2.086	0.111	0.102	1.04
Group #4	75/60/V/S	G4/2/NR	40	Yes	No	No	75	60	4.173	0.093	0.134	0.87
	75/60/V/S/WR	G4/2/4#4	36	Yes	Yes	No	75	60	2.151	0.098	0.119	0.48
	75/60/V/US	G4/3/NR	40	Yes	No	Yes	75	60	4.184	0.094	0.132	0.87
	75/60/V/US/WR	G4/3/4#4	39	Yes	Yes	Yes	75	60	2.164	0.102	0.131	0.93

[a] minimum flange width

[b] minimum flange thickness

[c] minimum web thickness

[d] minimum cross-section area

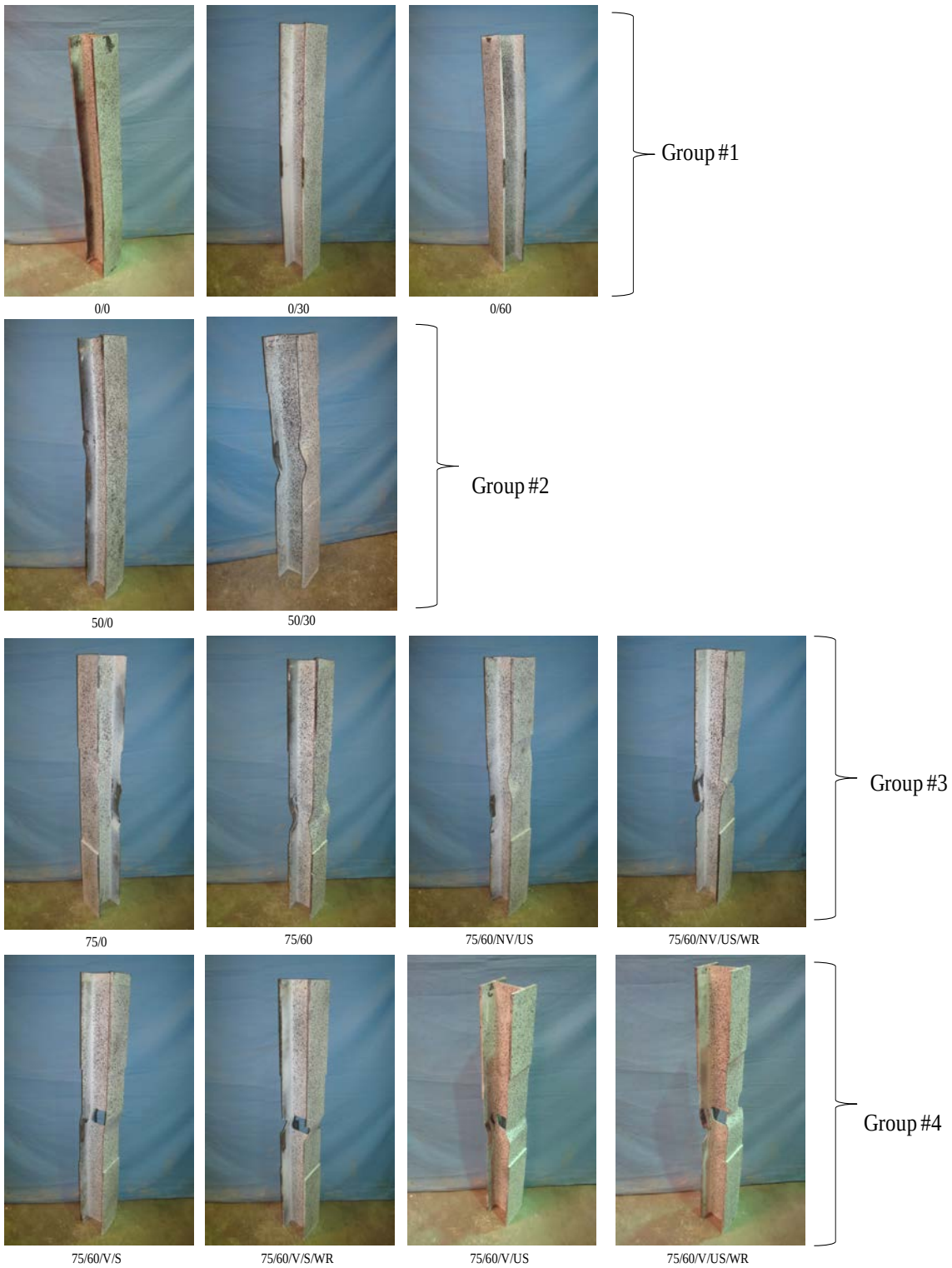

Figure 3.2. Failure Modes of Steel Piles before Repair (Karagah et al., 2013)

3.2 Manufacturer Reported Material Properties

The following materials were used to repair the specimens:

a) NS Grout: A non-shrink, non-staining, non-metallic Grout. Table 3.2 provides the properties of the grout as obtained from the manufacturer.

b) Gravel: An all-purpose gravel. It meets the ASTM C33-03 (2003) specifications. Washed and well-graded gravel.

c) GFRP: PileMedic PLG60.60. It is a high-strength FRP laminate constructed with bidirectional glass fabrics providing strength in both longitudinal and transverse direction. Table 3.3 shows the mechanical properties of the GFRP as obtained from the manufacturer.

d) Rebar: #3 and #4, 25 inches long grade 60.

e) Epoxy: QuakeWrap, QuakeBond J201TC Tack Coat. A two-part, high strength structural epoxy designed for vertical and overhead applications. Table 3.4 shows the properties of the epoxy as obtained from the manufacturer.

Table 3.2. Properties of Grout*

Property	Flowable Consistency 1.0 Gal/50 lb	Fluid Consistency 1.0 Gal/50 lb
Flow Rate	120%	20 to 30 seconds (flow cone)
Compressive Strength (2 in cubes)	3 days= 4.5 ksi	4 days= 3.5 ksi
	7 days= 6 ksi	8 days= 5 ksi
	28 days= 8.5 ksi	29 days= 6.8 ksi
Expansion	3 days= 0.01%	
	7 days= 0.03%	
	14 days= 0.05%	
	28 days= 0.05%	
Freeze- Thaw Resistance	300 cycles: 97%	NA
Setting Time	Initial Set= 3 hrs 5 min	
	Final Set= 4 hrs 47 min	

* http://www.euclidchemical.com/products/construction-products/grouts/cementitious/euco-pre-cast-grout/

Table 3.3. Properties of GFRP*

Longitudinal (0°) Direction:	
Tensile Strength	62 ksi
Modulus of Elasticity	3500 ksi
Ultimate Elongation	1.31%
Transverse (90°) Direction:	
Tensile Strength	60 ksi
Modulus of Elasticity	3650 ksi
Ultimate Elongation	1.06%
Laminate Properties	
Ply Thickness	0.26 in
Barcol Hardness	50 min
Water Absorption	0.8% max

* http://pilemedic.com/data/PileMedic%20PLG60.60.pdf

Table 3.4. Properties of Epoxy*

Full Cure Time	48 Hours
Density at 68° F (20° C)	Part A: 9.8 lbs/gal
	Part B: 9.4 lbs/gal
Tensile Strength	4.36 ksi
Tensile Modulus	329 ksi
Compressive Strength	8.006 ksi
Compressive Modulus	278.9 ksi
Flexural Strength	8.025 ksi
Flexural Modulus	250.1 ksi
Shear Strength	1.453 ksi
Water Absorption (% gain) in 24 hours	<1%
Expansion Coefficient [-40°-0° C]	$61.21*10^{-6}$ m/m °C
Expansion Coefficient [50° to 175° C]	$210.58*10^{-6}$ m/m °C

* http://quakewrap.com/product_data_sheets/J201TC.pdf

3.3 Material Test Results

Material tests include GFRP coupons, concrete cylinders, steel coupons, and steel reinforcing bars. GFRP material test, concrete material test and steel reinforcing bars were tested in this study. Structural steel material result was obtained from previous research.

3.3.1 GFRP Material Properties

Two thin flat strips of GFRP were tested to measure the modulus of elasticity in longitudinal (0º) and transverse (90º) directions. In addition, GFRP was tested in 45º direction to measure the shear modulus. Width and thickness of the GFRP coupons was measured at three locations to determine the cross sectional area. The GFRP coupons were nominally 5.8 inches long, 1 inch wide and 0.026 inches thick. Strain gauges were bonded on the face of the GFRP at the center of the coupons to measure longitudinal and transverse strains. Figure 3.3 shows the GFRP tension coupons. GFRP coupons were tested using a 110 kips servo-hydraulic MTS load frame. Table 3.5 presents the measured properties of GFRP.

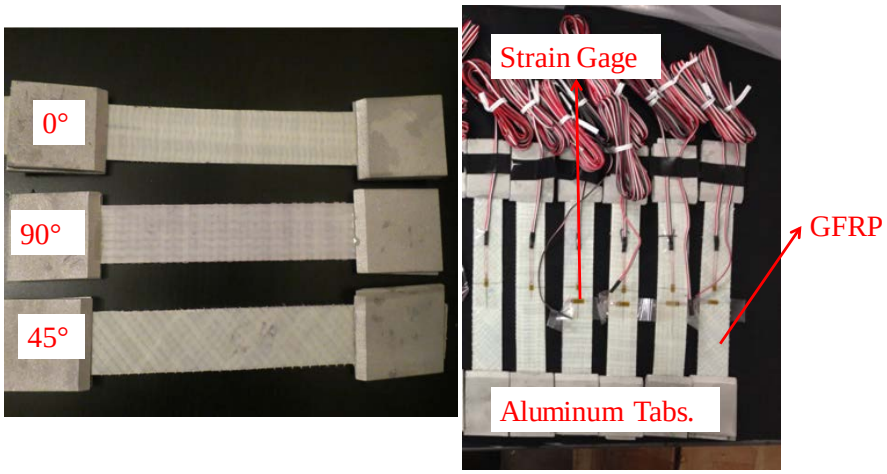

Figure 3.3. GFRP Coupons

Table 3.5. Mechanical Properties of GFRP

	Test 1	Test 2	Avg.
Tensile Strength (0°) Direction	55 ksi	46 ksi	50.5 ksi
Modulus of Elasticity (0°) Direction	2754 ksi	2700 ksi	2727 ksi
Tensile Strength (90°)Direction	47.6 ksi	55 ksi	51 ksi
Modulus of Elasticity (90°) Direction	3512 ksi	2707 ksi	3109 ksi
Maximum Shear Stress	5.47 ksi	-	5.47 ksi
Shear Modulus	566 ksi	-	566 ksi
Poisson's Ratio (ν_{12})*	0.19		
Poisson's Ratio (ν_{21})*	0.24		

* Poisson's Ratio (ν_{ij}): strain in the j-direction due to stress in the i-direction (1-direction is longitudinal direction, 2-direction is transverse direction

3.3.2 Structural Steel Material Properties

In order to determine the mechanical properties of the steel piles, six coupons, taken from web and flanges of the piles, were tested using a 400-kip Tinius-Olsen Universal Testing Machine as part of the previous testing of the unrepaired piles (Karagah et al., 2013). The mechanical properties of the structural steel are presented in Table 3.6. Coupons were tested according to ASTM A370-12a (2012).

Table 3.6. Mechanical Properties of the Steel Piles (Karagah et al., 2013)

Coupon Designation	Modulus of Elasticity	Yield Strength	Ultimate Strength	Strain at Ultimate Strength	Elongation at Failure
	(ksi)	(ksi)	(ksi)	(in/in)	(%)
Flange	26925	56.1	69.4	0.13301	29.5
Web	26085	63.7	76.8	0.06962	21.3

3.3.3 Rebar Material Properties

A series of tension tests were conducted to determine the mechanical properties of the reinforcing steel bars used in this study. A total of 4 coupons were tested according to ASTM A370-12 (2012). Two of the coupons are #3 rebar and two of them are #4 rebar.

The coupons were tested using a 110 kips servo-hydraulic MTS load frame. Axial strains were measured 6-inch axial extensometer. The specimens were loaded at displacement rates of 0.02 in/min respectively. The values of the mechanical properties are summarized in Table 3.7.

Table 3.7. Mechanical Properties of Rebar

Coupon Designation	Rebar #3			Rebar #4		
	Test 1	Test 2	Avg.	Test 1	Test 2	Avg.
Modulus of Elasticity (ksi)	27042	28050	27546	28666	28977	28821.5
Yield Strength (ksi)	60.9	65.9	63.4	58.9	56.9	57.9
Ultimate Strength (ksi)	79.6	96.5	88.05	97.5	96.2	96.9

3.3.4 Concrete Material Properties

Four batches of concrete were cast in the this study. To evaluate the compressive strength of the concrete, 4 × 8 inch cylinders were cast and cured with the test piles. The cylinders were tested following ASTM C39/C39M 03 (2003) in a 500-kip capacity Forney cylinder test frame. Loading was applied without shock. The cylinders that were tested on 8/5/2014, 8/9/2014, 8/1/2014 and 8/4/2014 were capped with sulfur while the other cylinders were tested with Neoprene rubber pads inserted in steel end caps. The cylinder test results are summarized in Table 3.8 and representative failed cylinders from each group are shown in Figure 3.4.

Table 3.8. Cylinder Test Results

Casting Group	Casting Date	Test Date of Cylinders	Test Date of Columns	Designation of Columns	Curing Days	Failure Load (kips)	Failure Stress (ksi)
Group #1	7/22/2014	8/5/2014	8/1/2014-8/7/2014	G1/2/NR-1, G1/2/NR-2, G2/3/NR-1, G2/3/NR-2	14	89	7.1
	7/22/2014	8/5/2014			14	90	7.2
	7/22/2014	8/9/2014			18	91	7.3
	7/22/2014	8/9/2014			18	93	7.4
	7/22/2014	8/9/2014			18	90	7.2
	7/22/2014	8/9/2014			18	97	7.8
	7/22/2014	8/9/2014			18	97	7.7
	7/22/2014	8/9/2014			18	96	7.6
	7/22/2014	8/9/2014			18	97	7.7
Group #2	6/9/2014	7/3/2014	7/2/2014-7/7/2014	G1/2/NR-3, G3/2/4#3-1, G4/2/NR	24	112	8.9
	6/9/2014	7/3/2014			24	110	8.8
	6/9/2014	7/8/2014			29	113	9.0
	6/9/2014	7/8/2014			29	119	9.5
	6/9/2014	7/8/2014			29	116	9.2
Group #3	1/30/2014	5/8/2014	5/8/2014-5/29/2014	G3/2/4#3-2, G3/3/4#3, G3/2/4#4	98	125	10.0
	1/30/2014	5/8/2014			98	128	10.2
	1/30/2014	5/9/2014			99	130	10.4
	1/30/2014	5/9/2014			99	136	10.8
	1/30/2014	5/29/2014			119	129	10.3
Group #4	7/7/2014	7/25/2014	7/25/2014-8/1/2014	G4/2/4#4, G4/3/NR, G4/3/4#4	18	106	8.4
	7/7/2014	8/1/2014			25	109	8.7
	7/7/2014	8/1/2014			25	106	8.4
	7/7/2014	8/4/2014			28	108	8.6

Figure 3.4. Failure of Cylinders A) Group #4, B) Group #3, C) Group #1 and #2

3.4 Fabrication of Test Specimens

The GFRP jackets that were used in this study were fabricated from a continuous flexible GFRP laminate that was wrapped around the pile and bonded to itself to produce a multi-layered closed, circular GFRP tube. The benefit of this system is that the GFRP tube can be manufactured on site to any length, diameter, and thickness desired to meet the demands of the specific repair application at hand. This overcomes several challenges associated with pre-fabricated GFRP jackets: (1) a large amount of material can be kept on hand ready to be mobilized immediately after damage is identified, (2) the jackets do not need to be fabricated to pre-specified dimensions making the system versatile and easy to mobilize, (3) if the materials are stockpiled, there is essentially no lead time required to fabricate the jackets facilitating rapid response.

The repair procedure included six steps.

(1) Steel piles had to be cleaned for proper adhesion between the concrete and steel. Epoxy, strain gages, and paint from prior testing of the piles had to be removed by metal brush and alcohol before repair.

(2) The next step was cutting the GFRP to an appropriate size. Fifty inches wide GFRP laminates were provided by the manufacturer. As will be mentioned later on the test matrix includes two and three layers of GFRP wrapping. Therefore, GFRP was cut with a wet saw into two sizes 25x59 inches and 25x84 inches (see Figure 3.5). An overlap of eight inches was used as recommended in the manufacturer's data sheet.

(3) The next step was preparing the wood spacers. Two inch diameter spacers were used to hold the GFRP jacket at right location while concrete was cast. Eight spacers were used for each specimen (see Figure 3.6). A five-minute epoxy was used to bond the spacers to the flanges of the steel piles. The spacers were permanently left inside the concrete.

(4) The GFRP laminates were sanded on both sides in one direction using a grade 220 sand paper to improve the bonding of the laminate layers (see Figure 3.7). Epoxy was prepared according to the product data-sheet. Table 3.9 shows the amounts used in mixing the two parts of the epoxy. The two parts were mixed with a low speed (400-600 rpm) mixing paddle for three minutes until a uniform color was achieved. After mixing, the epoxy was applied to the entire surface of one side of the GFRP laminates using a spatula. Special care was given to keep the epoxy thickness around 0.04 inches. The steel piles were wrapped with flexible GFRP laminates in two and three layers with an overlap

of eight inches. The jackets were secured using plastic zip ties for 48 hours while the epoxy cured (see Figure 3.8).

(5) #3 and #4 rebar were placed (depending on the specimen) inside the jackets (Figure 3.9).

(6) The last step was casting the grout into the GFRP jacket. Because of the limitations of the concrete mixer, specimens were divided into four groups. Table 3.10 shows the mixture proportions for each group and the number of 4x8 inch cylinders prepared for compression testing. Groups #2 and #3 were cast inside the laboratory while Groups #1 and #4 were cast outside. The concrete was mixed using a gravity-based mixer and cast into the GFRP jackets (see Figure 3.10). The following steps were followed in casting the specimens: mix the concrete and gravel until the particles are uniformly distributed, pour water slowly and mix the concrete for three minutes, quickly transport the mixed material to the casting area, pour the mixed material into the specimens in three phases by fill one-third of the GFRP jacket and tamping 25 times with a tamping rod and repeating for the remainder two-thirds in two steps, and fill 4x8 inch plastic cylinder molds with the mixed material for compression testing.

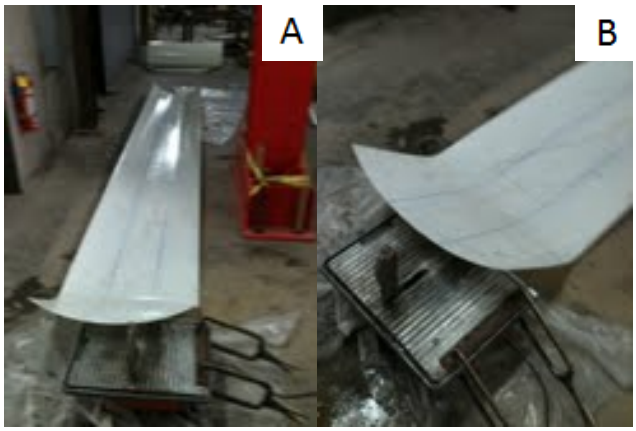

Figure 3.5. A) Cutting GFRP, B) Wet Saw

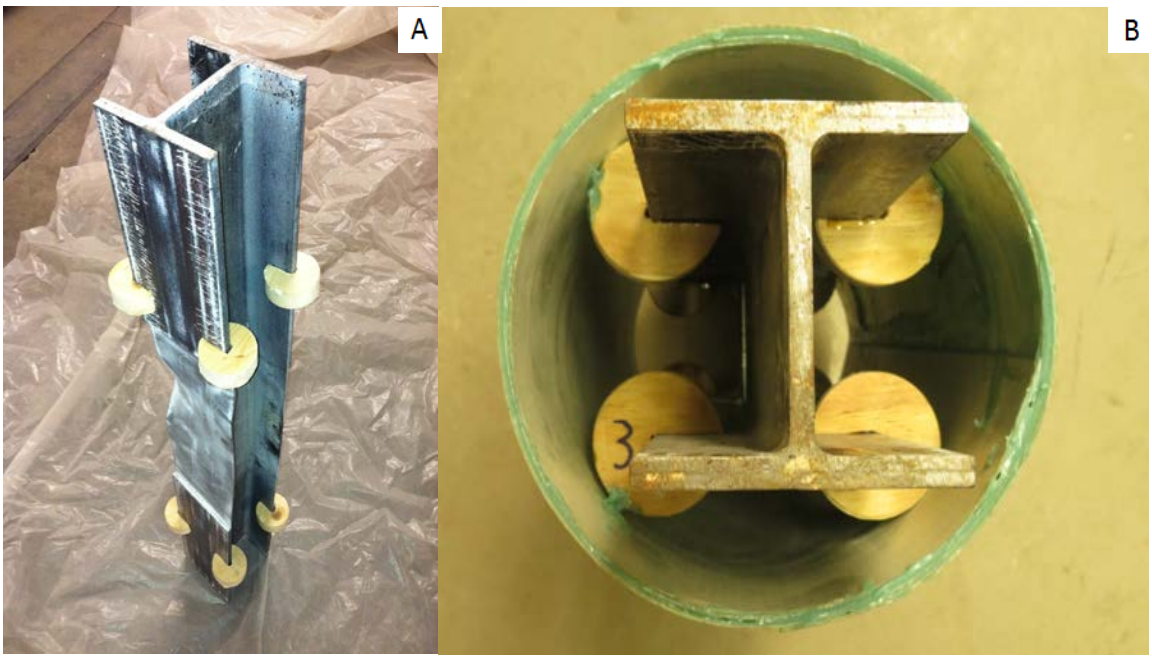

Figure 3.6. A) Spacers before Wrapping; B) Spacers after Wrapping

Figure 3.7. Sanding of the GFRP Laminates Using Sandpaper

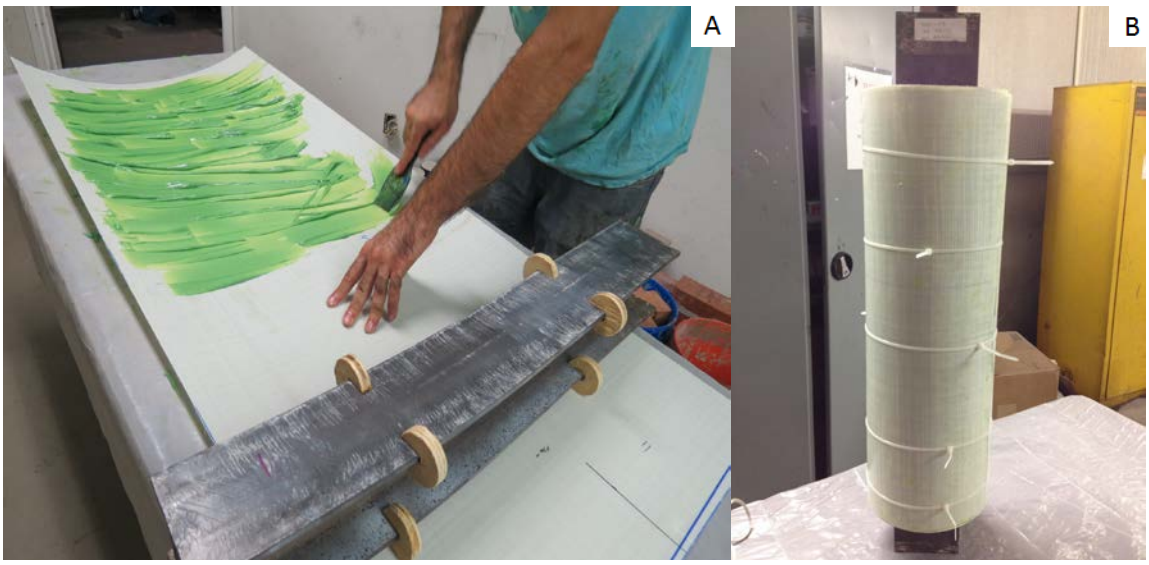

Figure 3.8. A) Application of Epoxy to GFRP laminates; B) Wrapped Steel Pile

Table 3.9. Components of Epoxy Mixing

Number of Layer	Component	
	A (lb)	B (lb)
2 Layers	0.97	0.47
3 Layers	1.68	0.8

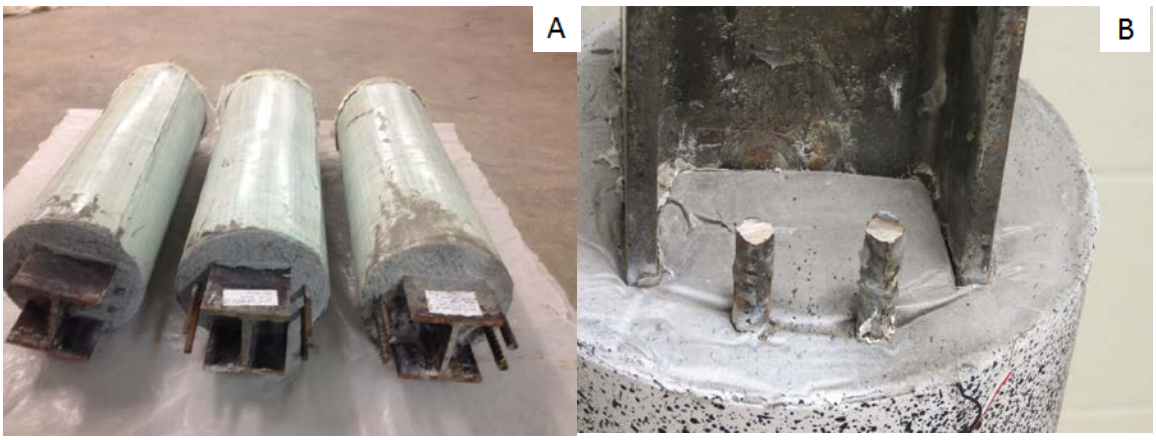

Figure 3.9. A) Location of Rebar, B) After Cutting

Table 3.10. Details of Mixing

Casting Group	Date of Casting	Grout (lbs)	Gravel (lbs)	Water (gal)	Total Volume (ft^3)	Number of Specimens	Number of Cylinders
Group #1	7/22/2014	325	162.5	6.5	3.9	4	9
Group #2	6/9/2014	275	137.5	4.95	3.3	3	5
Group #3	1/30/2014	250	125	4.37	3	3	6
Group #4	7/7/2014	275	137.5	4.95	3.3	3	5

Figure 3.10. Casting Concrete

3.5 Test Matrix

Table 3.11 shows the details of the repair applied on the test specimens. Twelve specimens had a length of 32 inches and one of the specimens was 27 inches long. Each of the specimens was designated with a label made up of three parts. The first part of the

label shows the group number. Note that the specimen grouping does not follow the casting number and the specimens were grouped based on their unrepaired axial strength from prior testing. The second part shows the number of GFRP layers. The third part denotes the number of reinforcing bars and size of the rebar if there is reinforcing bars inside of the GFRP jacket. As an example, G3/2/4#4 indicates that the specimen was in group three, two layers of GFRP were used, four reinforcing bars were placed inside the jacket and rebar size is #4. If exactly the same repair scheme is used for multiple specimens that were damaged to different levels in prior testing, a dash and a repetition number is added to the end of the third label part.

The repair length of the specimens was 25 inches with the exception that Specimen G2/3/NR-2 had a 20.5 inches repair length because it was only 27 inches long. Eight specimens were fabricated with two layers of GFRP. The remaining specimens were wrapped with three layers of GFRP. Additionally, four #3 rebar were used to repair three of the specimens and four #4 rebar were used to repair three of the specimens.

Figure 3.11 shows the plan of the repair system. The diameter of the GFRP jacket was 8 inches. There was an unrepaired area on both ends of the specimens that is 3.5 inches long.

Table 3.11. Test Matrix

	Designation		Length (in)	Section	Retrofitting Length (in)	Retrofitting Scheme	FRP Layer	Rebar #3	Rebar #4
	Karagah et al. (2013)	This Study							
Group #1	0/0	G1/2/NR-1	32	W4X13	25	Grout + GFRP	2	-	-
	0/30	G1/2/NR-2	32	W4X13	25	Grout + GFRP	2	-	-
	0/60	G1/2/NR-3	32	W4X13	25	Grout + GFRP	2	-	-
Group #2	50/0	G2/3/NR-1	32	W4X13	25	Grout + GFRP	3	-	-
	50/30	G2/3/NR-2*	27	W4X13	20.5	Grout + GFRP	3	-	-
Group #3	75/0	G3/2/4#3-1	32	W4X13	25	Grout + GFRP + Rebar	2	4	-
	75/60	G3/2/4#3-2	32	W4X13	25	Grout + GFRP + Rebar	2	4	-
	75/60/NV/US	G3/3/4#3	32	W4X13	25	Grout + GFRP + Rebar	3	4	-
	75/60/NV/US/WR	G3/2/4#4	32	W4X13	25	Grout + GFRP + Rebar	2	-	4
Group #4	75/60/V/S	G4/2/NR	32	W4X13	25	Grout + GFRP	2	-	-
	75/60/V/S/WR	G4/2/4#4	32	W4X13	25	Grout + GFRP + Rebar	2	-	4
	75/60/V/US	G4/3/NR	32	W4X13	25	Grout + GFRP	3	-	-
	75/60/V/US/WR	G4/3/4#4	32	W4X13	25	Grout + GFRP + Rebar	3	-	4

* Total length= 27 inches; repaired length= 20.5 inches

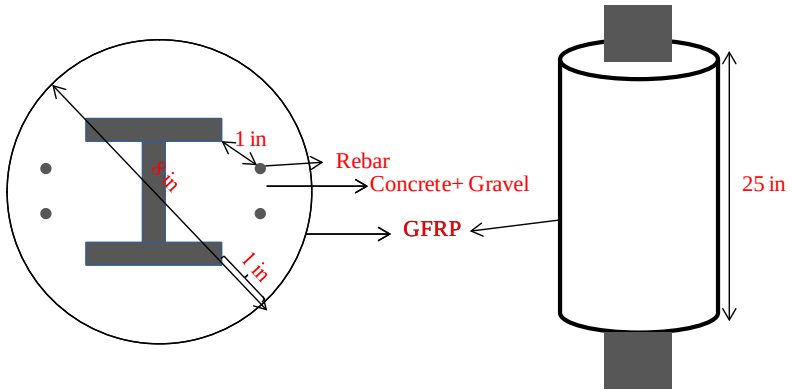

Figure 3.11. Plan of Repaired Specimen

3.6 Test Setup

The specimens were tested under monotonic compression load using a 400 kips capacity Tinius-Olsen Universal Testing Machine. The boundary conditions of the piles were designed to provide a nominally simply-supported condition about the weak axis of the pile and a nominally fixed/pinned condition about the strong axis. A thin layer of plaster was applied at the end caps to fill the gap between the specimen and the support plate (see Figure 3.12). Figure 3.13 shows the test setup, including the testing frame and the data acquisition system (Vishay Micro-Measurements System 7000). View of a test specimen is showed in Figure 3.13.

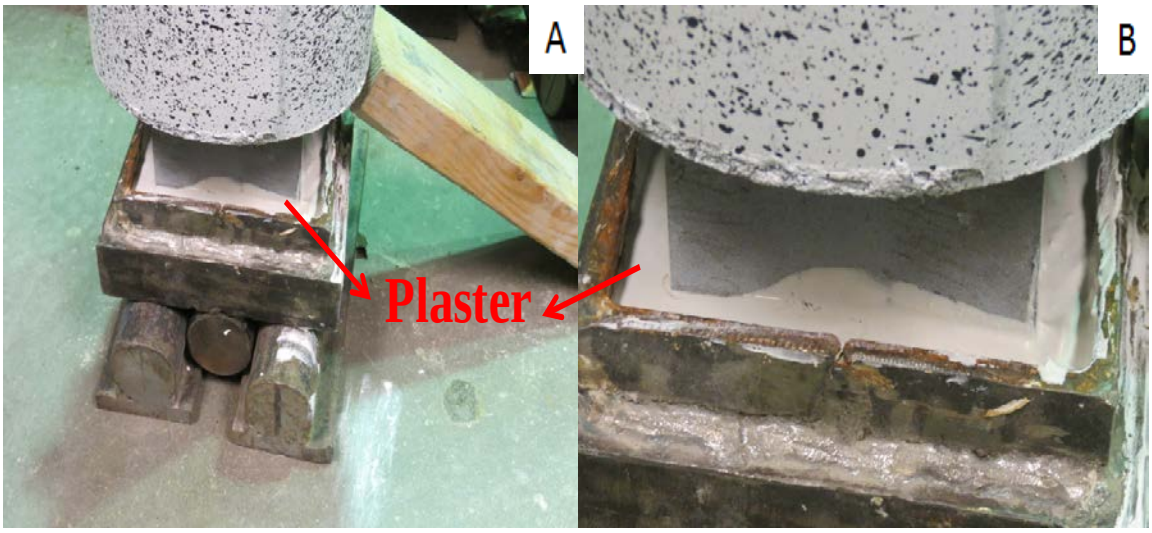

Figure 3.12. Plaster Applied to the End Caps

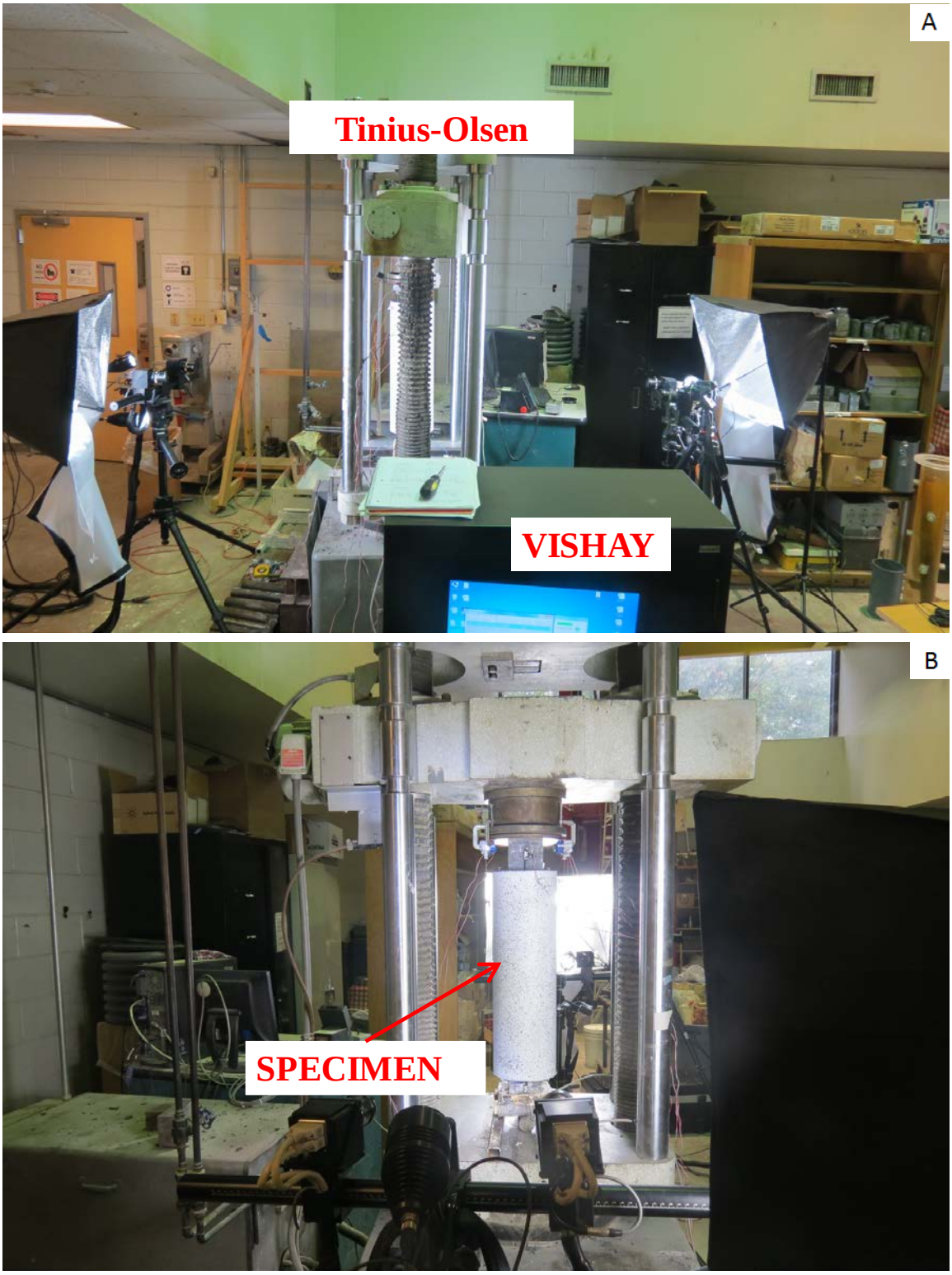

Figure 3.13. A) Test Setup, B) View of a Test Specimen

3.7 Instrumentation

Two types of sensors were used in the experiments: Linear potentiometers that were string type or plunger type and strain gages. Figure 3.14 shows the location of linear and string potentiometers. Two different plunger type linear potentiometers were used with 0.5 and 1.0 inch stroke to determine the slip between the steel pile and the concrete filled GFRP jacket. The 1.0 inch stroke linear potentiometers were placed on top while the 0.5 inch stroke potentiometers were placed on the bottom (see Figure 3.16). These linear potentiometers were placed on the flanges (one on each side) of the specimens as shown in Figure 3.15 and Figure 3.16. Four string potentiometers were placed at the four corners of each specimen to measure the axial shortening. The string potentiometers were installed in such a manner so as to measure the linear displacement between the two end caps. Each of the sensors mentioned above were calibrated before the test. Specimens were also instrumented with strain gages. Eight strain gages were used for specimen G3/2/4#3-2 and four strain gages were used for the others. The results from the strain gages did not provide further insight on the pile behavior; therefore, they are not discussed in detail here. Appendix A shows the results and locations of the strain gages.

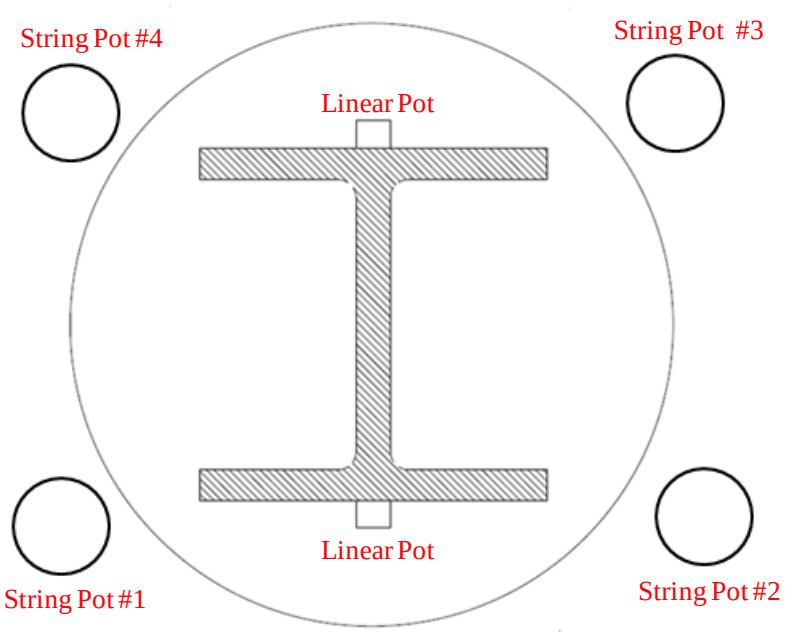

Figure 3.14. Locations of Linear and String Potentiometers

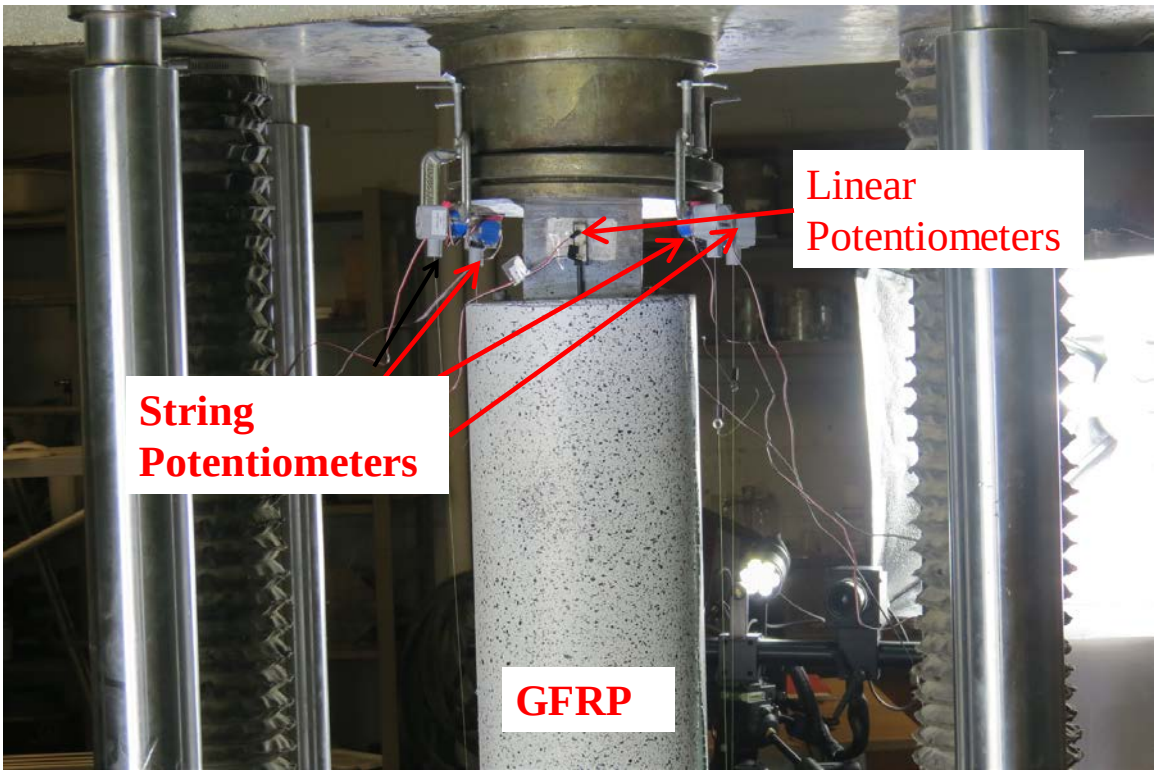

Figure 3.15. Top End Cap, String Potentiometers and Linear Potentiometers

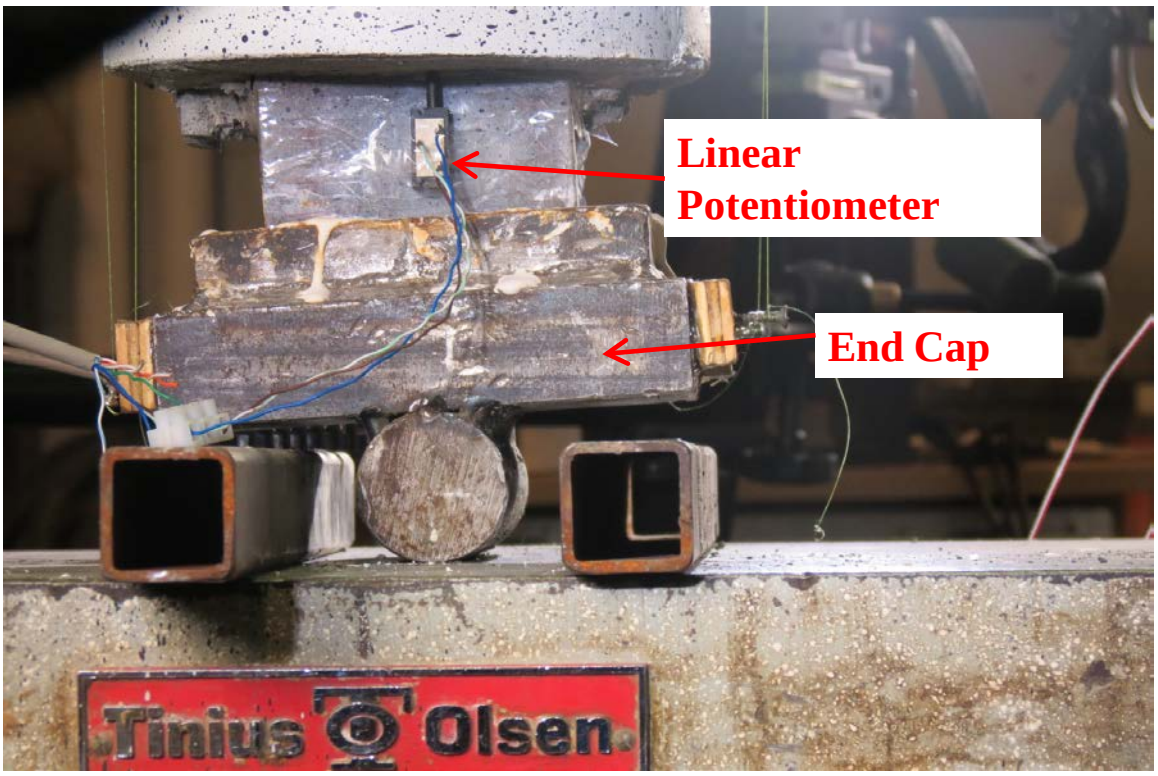

Figure 3.16. Bottom End Cap Showing 0.5 inch Stroke Linear Potentiometers

3.8 Loading Protocol

All specimens were subjected to the same loading protocol. Before starting the test, all sensors were checked to verify that they are functioning properly. Vishay data acquisition system and the Tinius-Olsen test frame were synchronized manually by starting them simultaneously. After the tests, the readings of all the systems were more precisely synchronized by comparing the load and displacement readings at least one of which was recorded on all of the systems. Until 300 lb of loading, a displacement ramp rate of 0.2 inch/min was used. It was assumed that the actual loading of the specimens started at 300 lb while the earlier stages were considered as seating of the specimens. When the load reached 300 lb the force was held constant for two minutes to check the systems one more time. After that the ramp rate was decreased to 0.008 inch/min and

held constant until the completion of the tests. The tests were stopped when specimen failure or excessive lateral deformations were observed.

4 Experimental Results

This chapter presents the experimental results of all 13 repaired piles. The piles were grouped into four according to their maximum strength as obtained from previous research (see Table 3.1 and Table 4.1).

Table 4.1. Groups of Specimens

Group #1		Group #2	
Karagah et al. (2013)	This Study	Karagah et al. (2013)	This Study
0/0	G1/2/NR-1	50/0	G2/3/NR-1
0/30	G1/2/NR-2	50/30	G2/3/NR-2
0/60	G1/2/NR-3		
Group #3		**Group #4**	
Karagah et al. (2013)	This Study	Karagah et al. (2013)	This Study
75/0	G3/2/4#3-1	75/60/V/S	G4/2/NR
75/60	G3/2/4#3-2	75/60/V/S/WR	G4/2/4#4
75/60/NV/US	G3/3/4#3	75/60/V/US	G4/3/NR
75/60/NV/US/WR	G3/2/4#4	75/60/V/US/WR	G4/3/4#4

4.1 Behavior of Piles in Group #1

Prior to repair, all the piles in Group #1 failed by global buckling at load levels varying from 178 to 215 kips. After reaching their peak loads, loading of the piles continued until the load decreased to levels between 91 and 182 kips. Figure 4.1 presents the axial load- displacement relationships of the damaged piles prior to repair with the GFRP-based system. The piles were repaired and tested as described in Chapter 3.

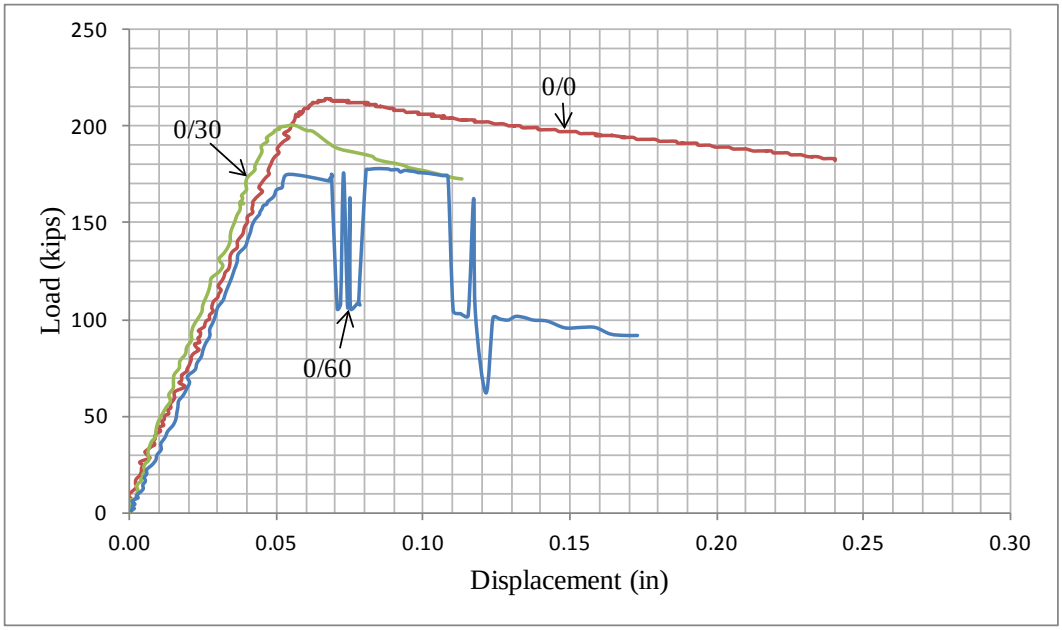

Figure 4.1. The Axial Load-Displacement Relationships of the Damaged Piles in Group #1

Pile G1/2/NR-1 failed at a load level of 202 kips due to buckling of the pile and rupture of the GFRP as illustrated in Figure 4.2. Prior to the repair, the control pile failed by global buckling at a load level of 215 kips. The capacity of the repaired pile was 94% of the capacity of the undamaged control pile. Figure 4.3 compares the axial load-shortening responses of the control pile (prior to repair) and the repaired buckled pile (after installation of the jacket).

Pile G1/2/NR-2 failed at a load level of 204 kips due to buckling of the pile and rupture of GFRP as illustrated in Figure 4.4 Prior the repair, the column failed by global buckling a load level of 201 kips. The capacity of the repaired pile was approximately the same as the capacity of the damaged pile and 95% of the capacity of the undamaged control pile. Figure 4.5 compares the axial load-shortening responses of the corroded pile

(prior to repair) and the repaired buckled pile (after installation of the jacket) to the response of the undamaged control pile.

Pile G1/2/NR-3 failed at a load level of 212 kips due to GFRP rupture as illustrated in Figure 4.6. Prior to the repair, the pile failed by global buckling at a load level of 178 kips. After the peak load, the specimen continued to deform extensively and rupture of the GFRP was observed. The capacity of the repaired pile was 1.2 times the capacity of the damaged pile and 99% of the capacity of the undamaged control pile. Figure 4.7 compares the axial load-shortening responses of the corroded pile (prior the repair) and the retrofitted buckled pile (after installation of the jacket) to the response of the undamaged control pile. The irregular response of pile 0/60 during prior testing was attributed to the electro-magnetic interference and is not believed to represent the actual response of the pile.

Figure 4.8 presents the slip behavior for specimens G1/2/NR-1, G1/2/NR-2, and G1/2/NR-3. In addition, the entire first group specimens are compared in Figure 4.9 before and after repair.

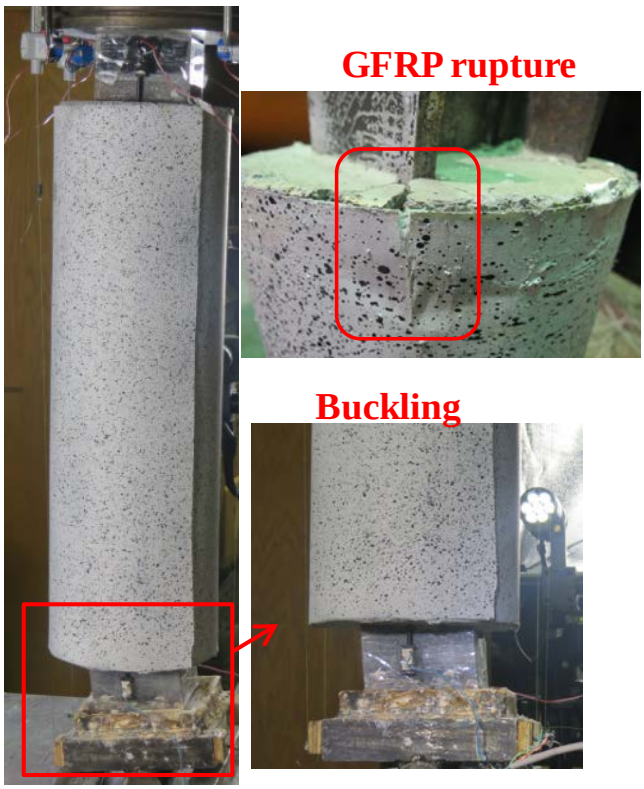

Figure 4.2. Failure of G1/2/NR-1

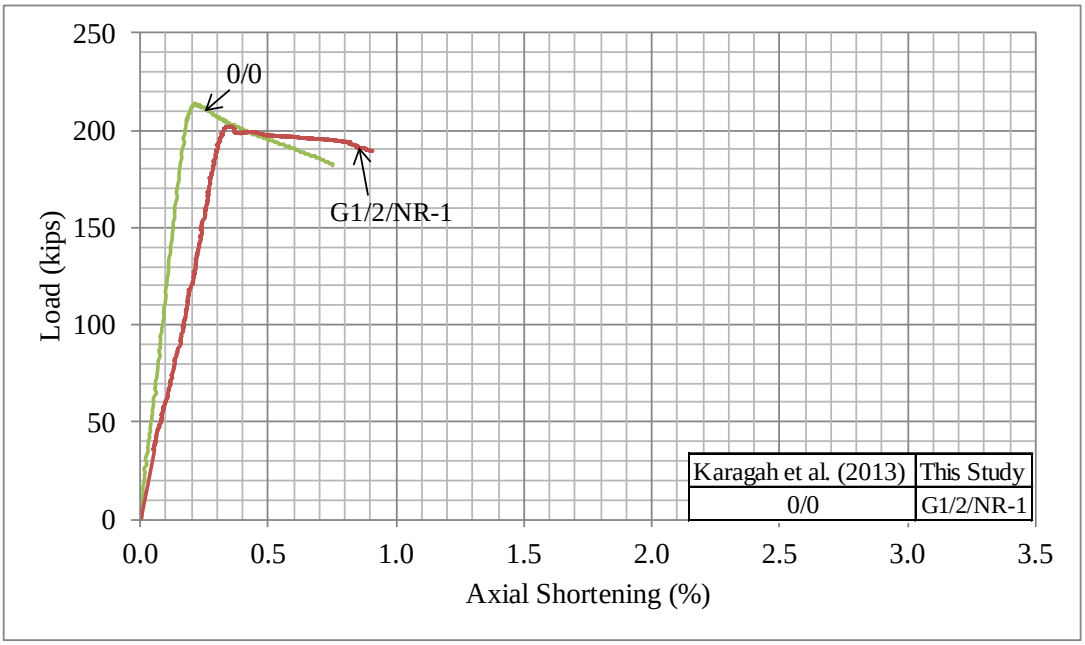

Figure 4.3. Load versus Axial Shortening of G1/2/NR-1

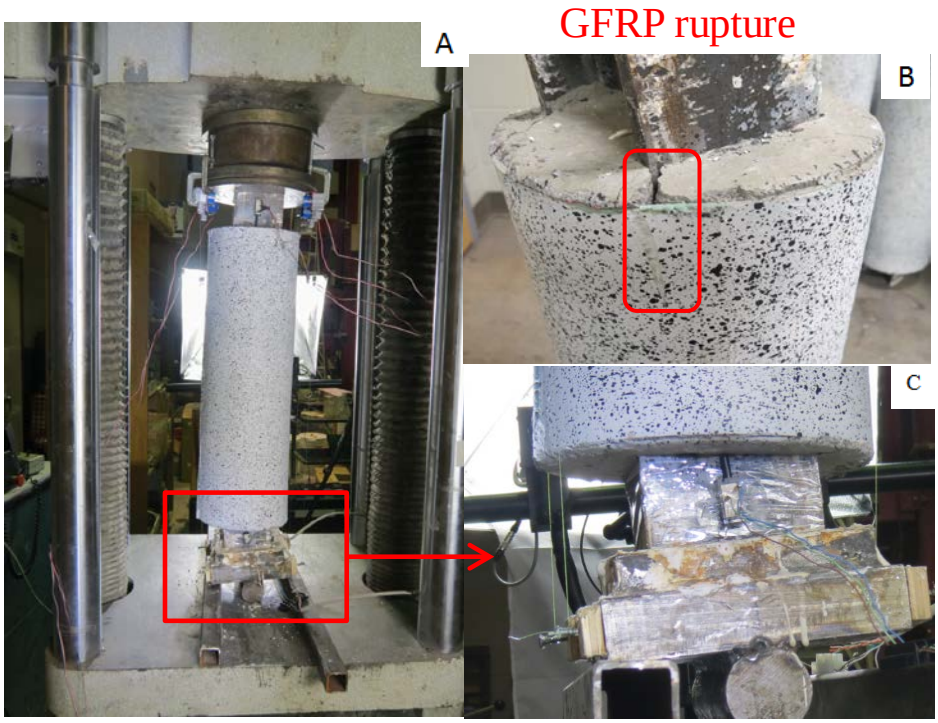

Figure 4.4. A) Failure of G1/2/NR-2, B) GFRP Rupture, C) Buckling

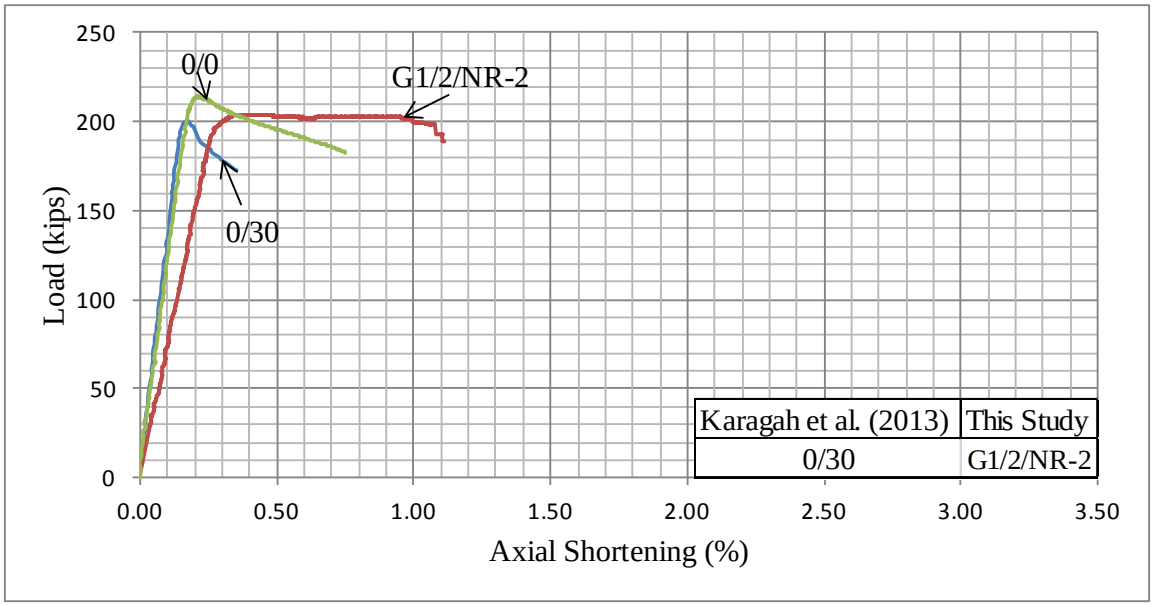

Figure 4.5. Load versus Axial Shortening of G1/2/NR-2

Figure 4.6. A) Failure of G1/2/NR-3, B) Buckling, C) GFRP Rupture

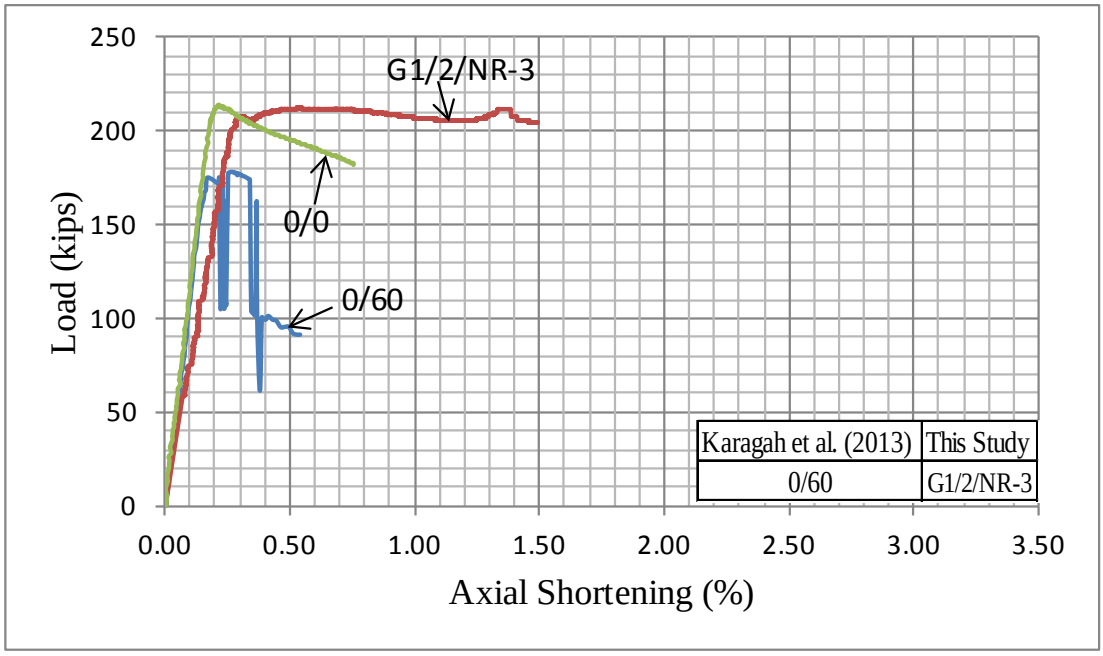

Figure 4.7. Load versus Axial Shortening of G1/2/NR-3

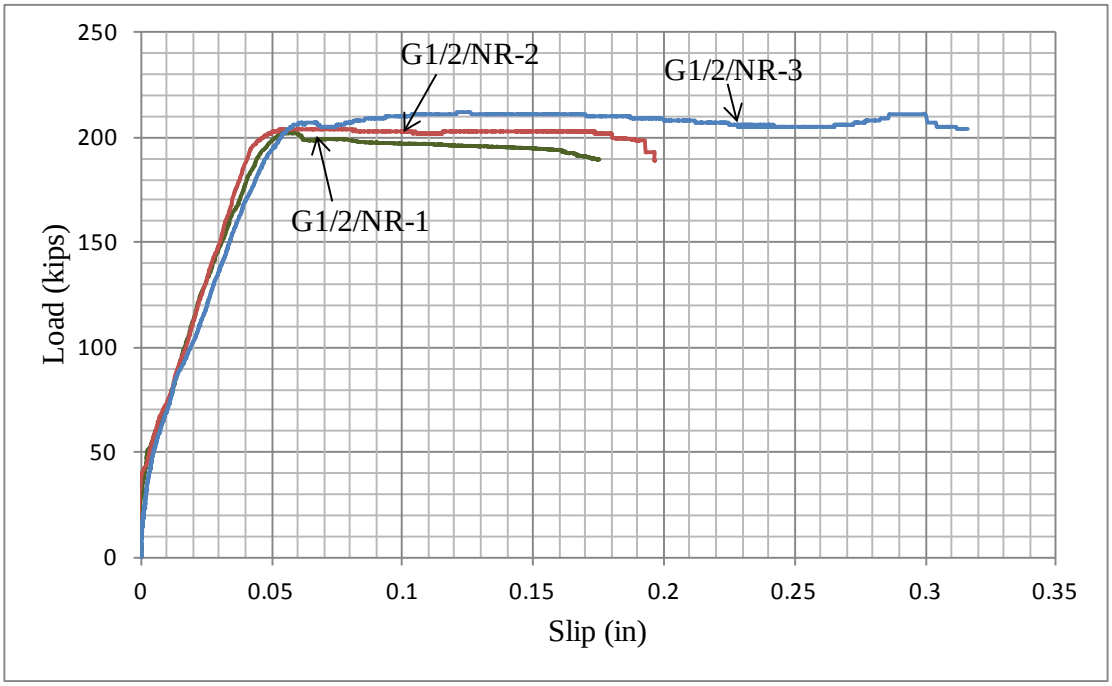

Figure 4.8. Load versus Slip Responses of G1/2/NR-1, G1/2/NR-2, and G1/2/NR-3

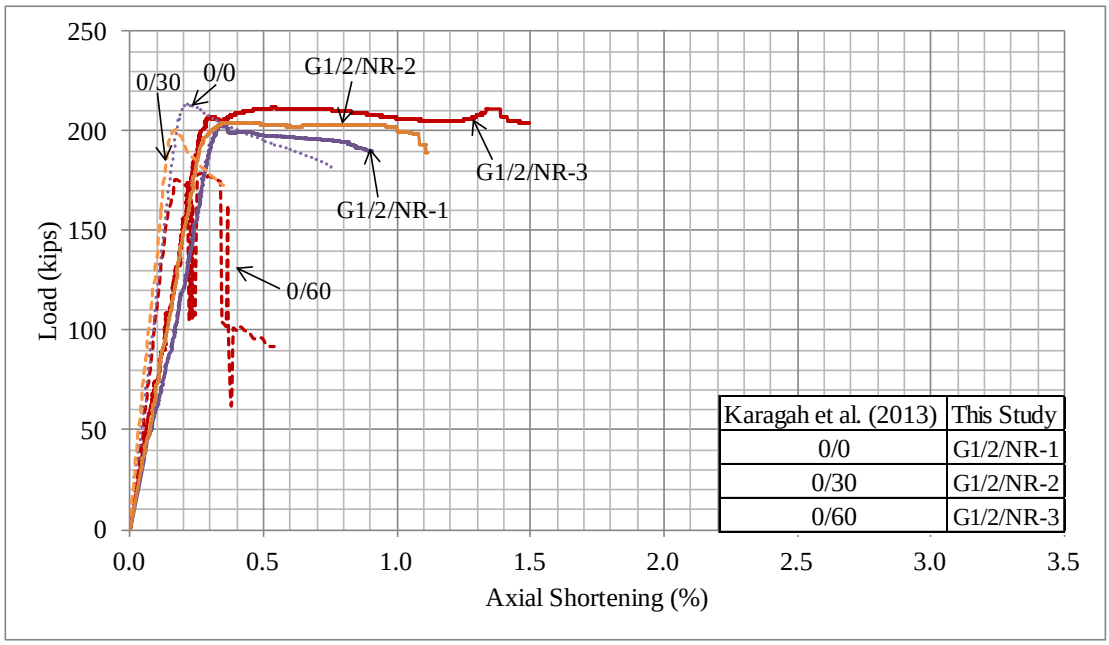

Figure 4.9. A) Load versus Shortening of All First Group Specimens

4.2 Behavior of Piles in Group #2

Prior to repair, the pile 50/0 failed by flange local buckling and pile 50/30 failed by flange and web local buckling at load levels of 117 and 130 kips, respectively. After reaching their peak loads, loading of the piles continued until the load decreased to 92 and 84 kips, respectively for piles 50/0 and 50/30. Figure 4.10 presents the axial load-displacement relationships of the damaged piles prior to repair with the GFRP-based system.

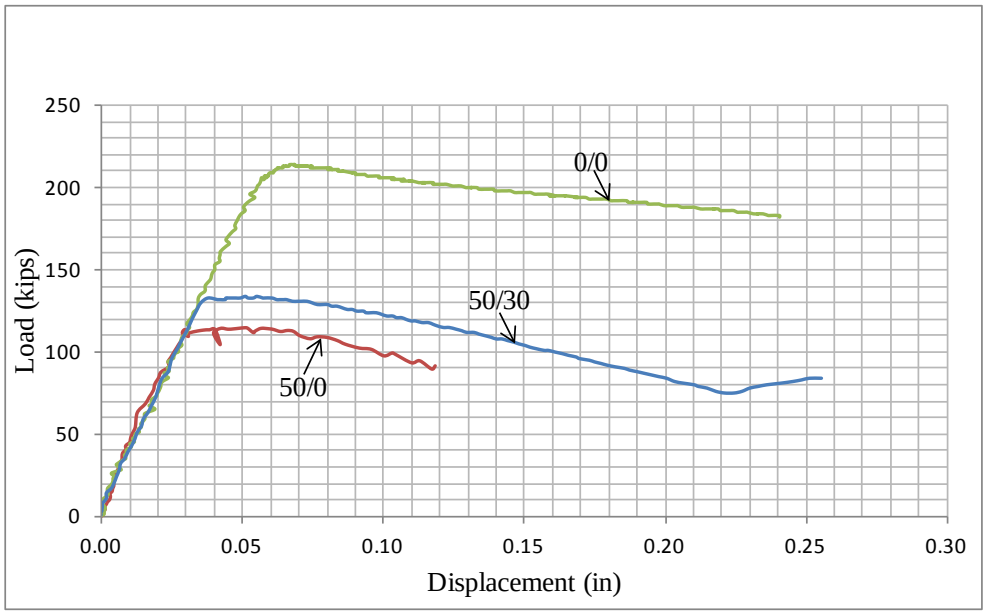

Figure 4.10. The Axial Load versus Displacement Relationships of the Damaged Piles in Group #2

Pile G2/3/NR-1 failed at a load level of 216 kips due to buckling of the pile and rupture of GFRP as illustrated in Figure 4.11. Prior to the repair, the pile failed by flange local buckling at a load level of 117 kips. The capacity of repaired pile was 1.8 times the capacity of the damaged pile and approximately equal to the capacity of the undamaged control pile. Figure 4.12 compares the axial load- shortening responses of the corroded

pile (prior to repair) and the repaired buckled pile (after installation of the jacket) to the response of the undamaged control pile.

Pile G2/3/NR-2 failed at a load level of 197 kips due to buckling of the pile and rupture of GFRP as illustrated in Figure 4.13. Prior to the repair, the pile failed by flange and web local buckling at a load level of 130 kips. The capacity of the repaired pile was 1.5 times the capacity of the damaged pile and 92% of the capacity of the undamaged control pile. Figure 4.14 compares the axial load-shortening responses of the corroded pile (prior to repair) and the repaired buckled pile (after installation of the jacket) to the response of the undamaged control pile.

The slip between steel and concrete for G2/3/NR-1 and G2/3/NR-2 is shown in Figure 4.15. The slip was not equal to zero because the steel piles were damaged already and the shortening of the piles was larger than the shortening of the jacket. The loads versus shortening responses of all the specimens Group#2 are presented in Figure 4.16.

Figure 4.11. Failure of G2/3/NR-1

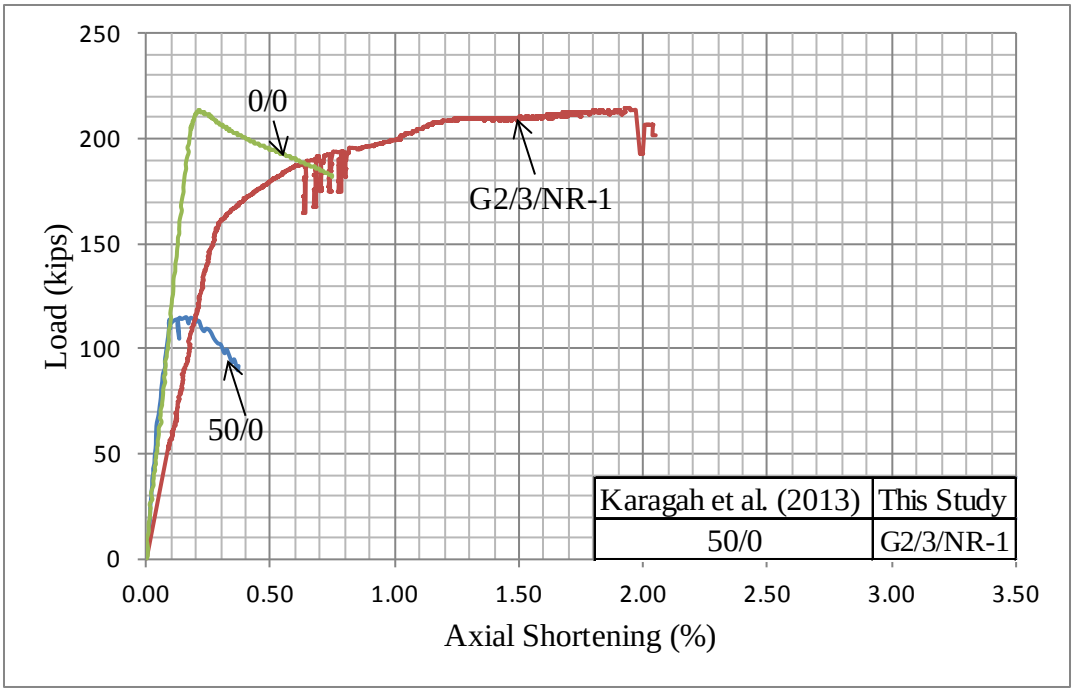

Figure 4.12. Load versus Axial Shortening of G2/3/NR-1

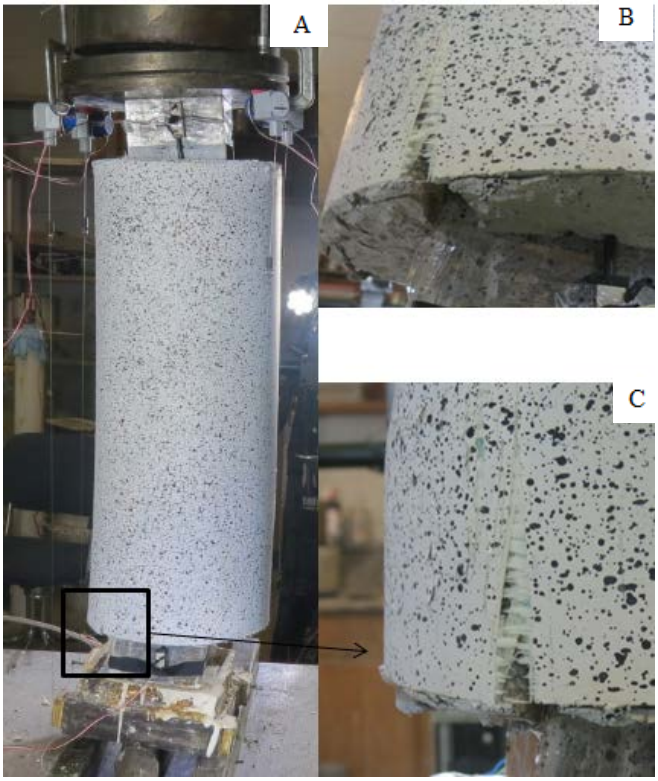

Figure 4.13. A) Failure of G2/3/NR-2, B) and C) GFRP Rupture

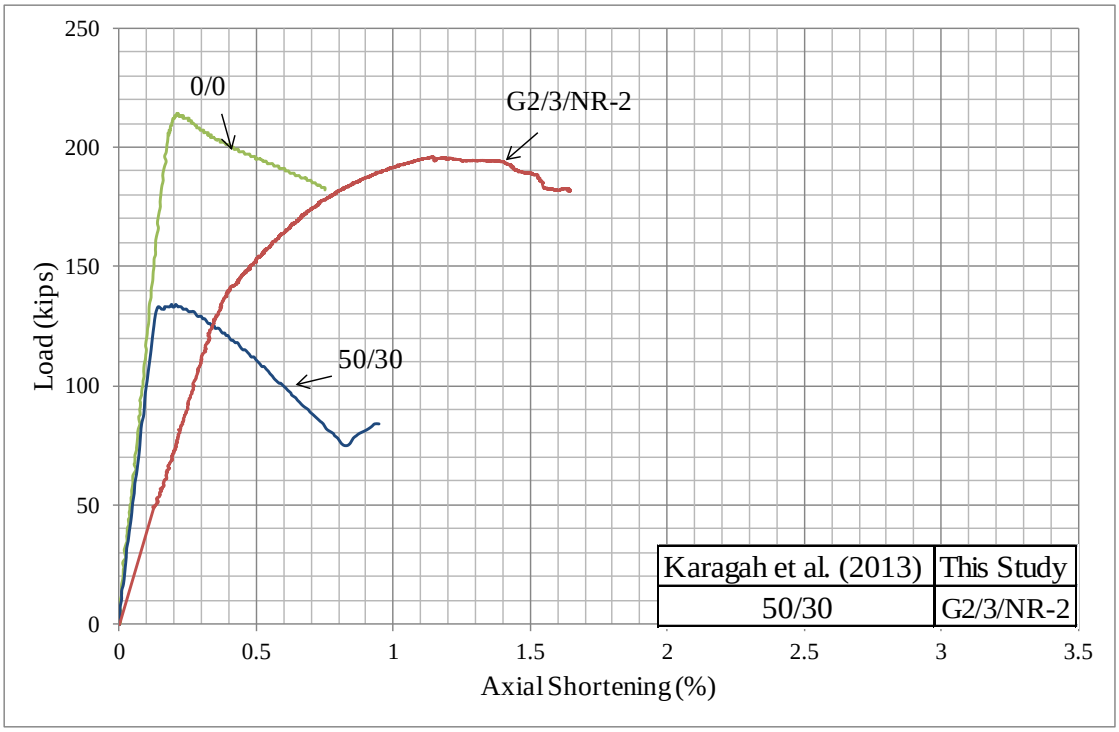

Figure 4.14. Load versus Axial Shortening of G2/3/NR-2

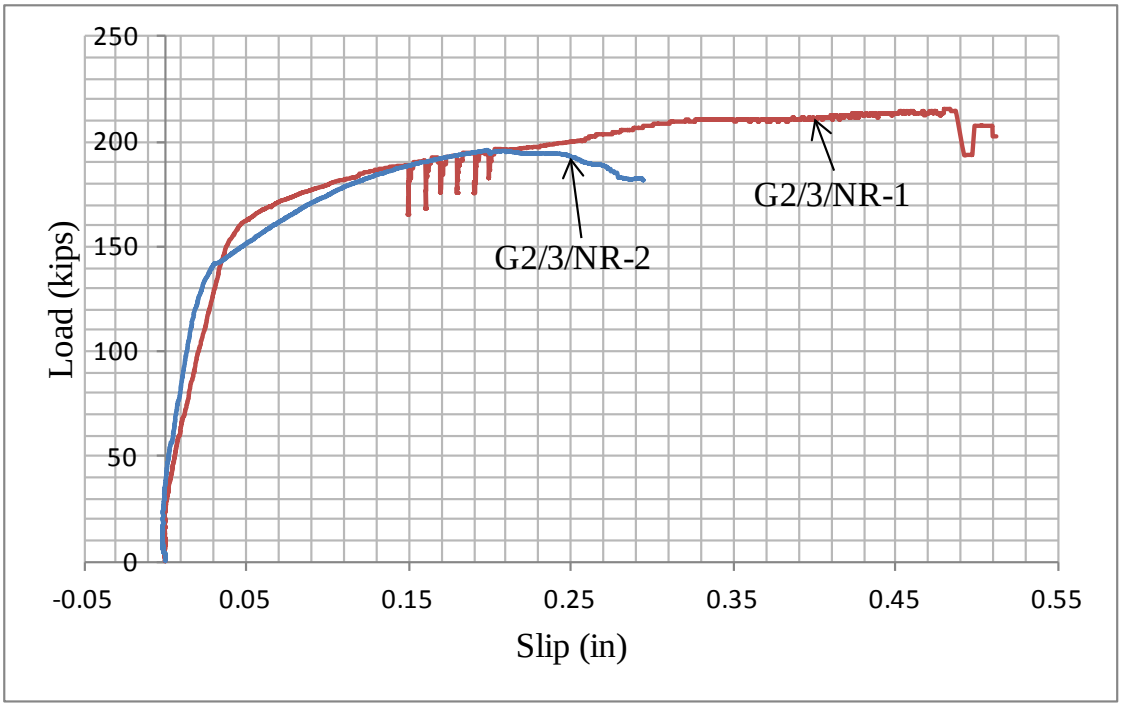

Figure 4.15. Load versus Slip Responses of G2/3/NR-1 and G2/3/NR-2

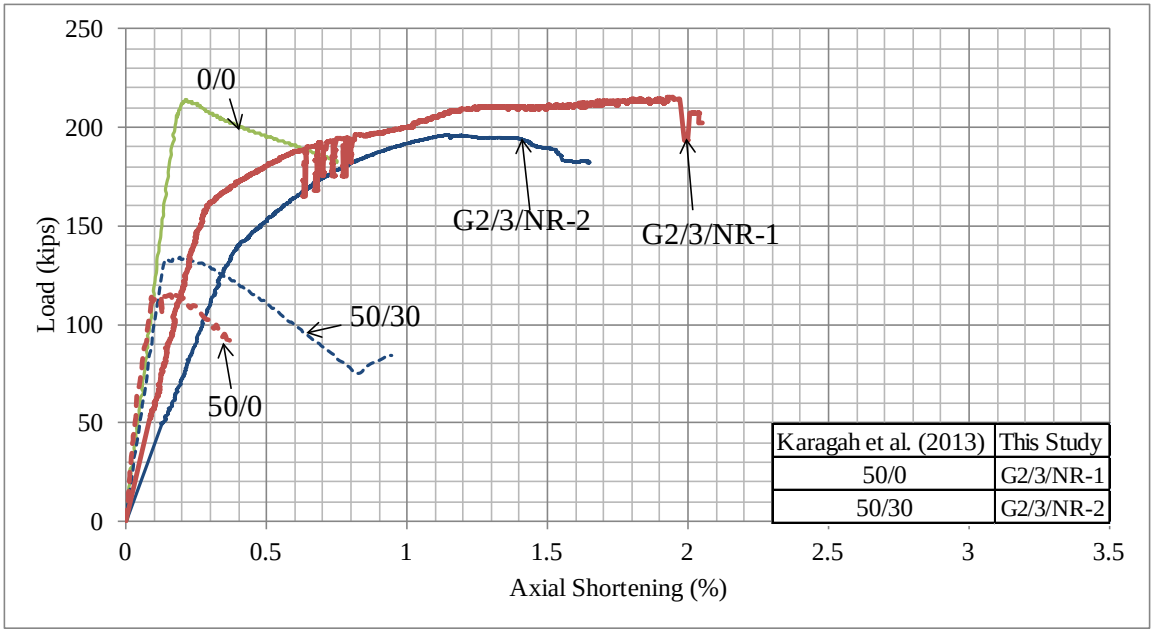

Figure 4.16. Load versus Shortening of Specimens in Group#2

4.3 Behavior of Piles in Group #3

Prior to repair, all the piles in Group #3 failed by flange and web local buckling at load levels varying from 57 to 92 kips. After reaching their peak loads, loading of the piles continued until the load decreased to levels between 39 and 73 kips. Figure 4.17 presents the axial load-displacement relationships of the damaged piles prior to repair with the GFRP-based system.

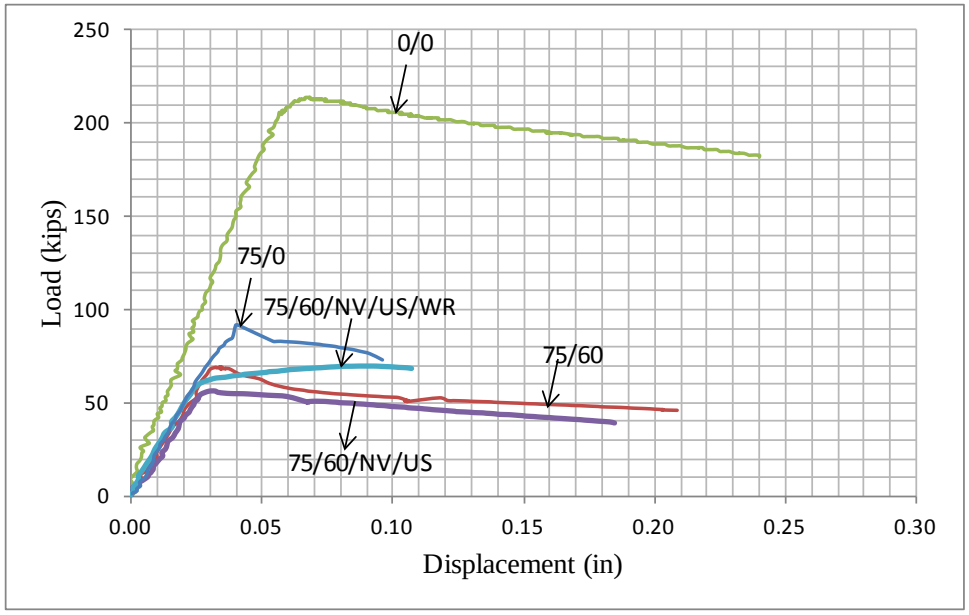

Figure 4.17. The Axial Load versus Displacement Relationships of the Damaged Piles in Group#3

Pile G3/2/4#3-1 failed at a load level of 205 kips due to GFRP rupture as illustrated in Figure 4.18. Prior to the repair, the pile failed by flange local buckling a load level of 92 kips. After the repair, failure mode was GFRP rupture near the mid-height of the pile. The capacity of the repaired pile was 2.2 times the capacity of the damaged pile and 95% of the capacity of the undamaged control pile. Figure 4.19 compares the axial load-shortening responses of the corroded pile (prior to repair) and the repaired buckled pile (after installation of the jacket) to the response of the undamaged control pile.

Pile G3/2/4#3-2 failed at a load level of 164 kips due to debonding of the GFRP initiating from the free end of the jacket as illustrated in Figure 4.20. This suggests that the sanding of the GFRP laminate was not sufficient to provide adequate bond between subsequent layers of the jacket. Upon inspection of the failed pile and removal of the GFRP, a rupture failure was observed in the inner layers the jacket. The capacity of the

repaired pile was 2.3 times the capacity of the damaged pile and 77% of the capacity of the undamaged control pile. Figure 4.21 compares the axial load-shortening responses of the corroded pile (prior to repair) and the repaired buckled pile (after installation of the jacket) to the response of the undamaged control pile.

Pile G3/2/4#4 failed at a load level of 210 kips due to GFRP rupture as illustrated in Figure 4.20. Prior to the repair, the pile failed by flange and web local buckling at a load level of 70 kips. The capacity of the repaired pile was 3 times the capacity of the damaged pile and 98% of the capacity of the undamaged control pile. Figure 4.22 compares the axial load-shortening responses of the corroded pile (prior to repair) and the repaired buckled pile (after installation of the jacket) to the response of the undamaged control pile.

Pile G3/3/4#3 failed at a load level of 223 kips due to global buckling of the pile which caused increased internal pressure on the concrete, resulting in higher slip between the steel and concrete and crushing of concrete as illustrated in Figure 4.20. The specimen buckled before the axial load reached the GFRP rupture level. Prior to the repair, the pile failed by flange and web local buckling at a load level of 57 kips. The capacity of the repaired pile was 3.9 times the capacity of the damaged pile and 104% of the capacity of the undamaged control pile. Figure 4.23 compares the axial load-shortening responses of the corroded pile (prior to repair) and the repaired buckled pile (after installation of the jacket) to the response of the undamaged control pile. Higher axial displacements were achieved in the repaired piles without a significant loss in the axial load carrying capacity due to buckling resistance provided by the concrete-filled jacket.

Figure 4.24 shows the slip between steel and concrete for specimens G3/2/4#3-1, G3/2/4#4 and G3/3/4#3. No slip data was obtained for specimen G3/2/4#3-2. In addition, load versus shortening response of all specimens in Group #3 are presented in Figure 4.25.

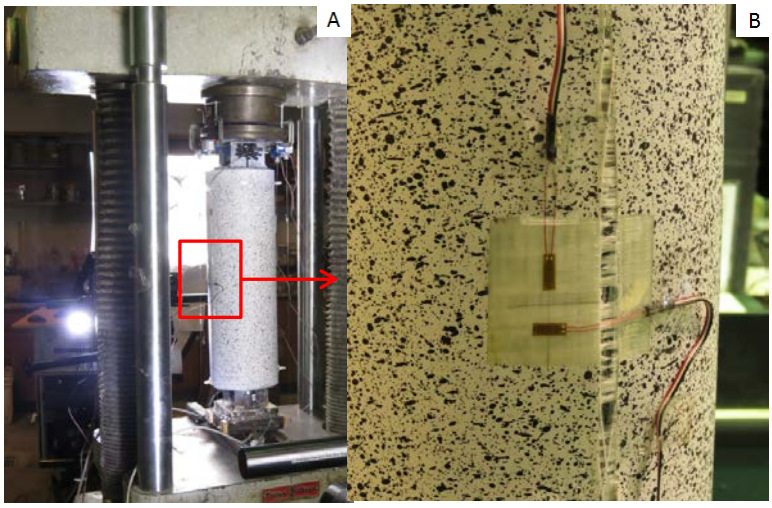

Figure 4.18. A) Failure of G3/2/4#3-1, B) GFRP Rupture

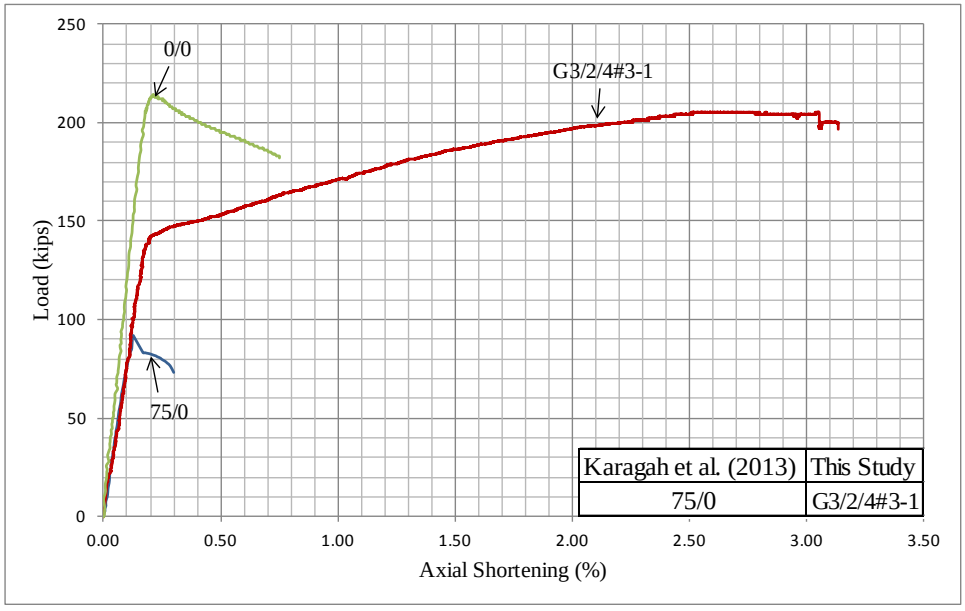

Figure 4.19. Load versus Axial Shortening of G3/2/4#3-1

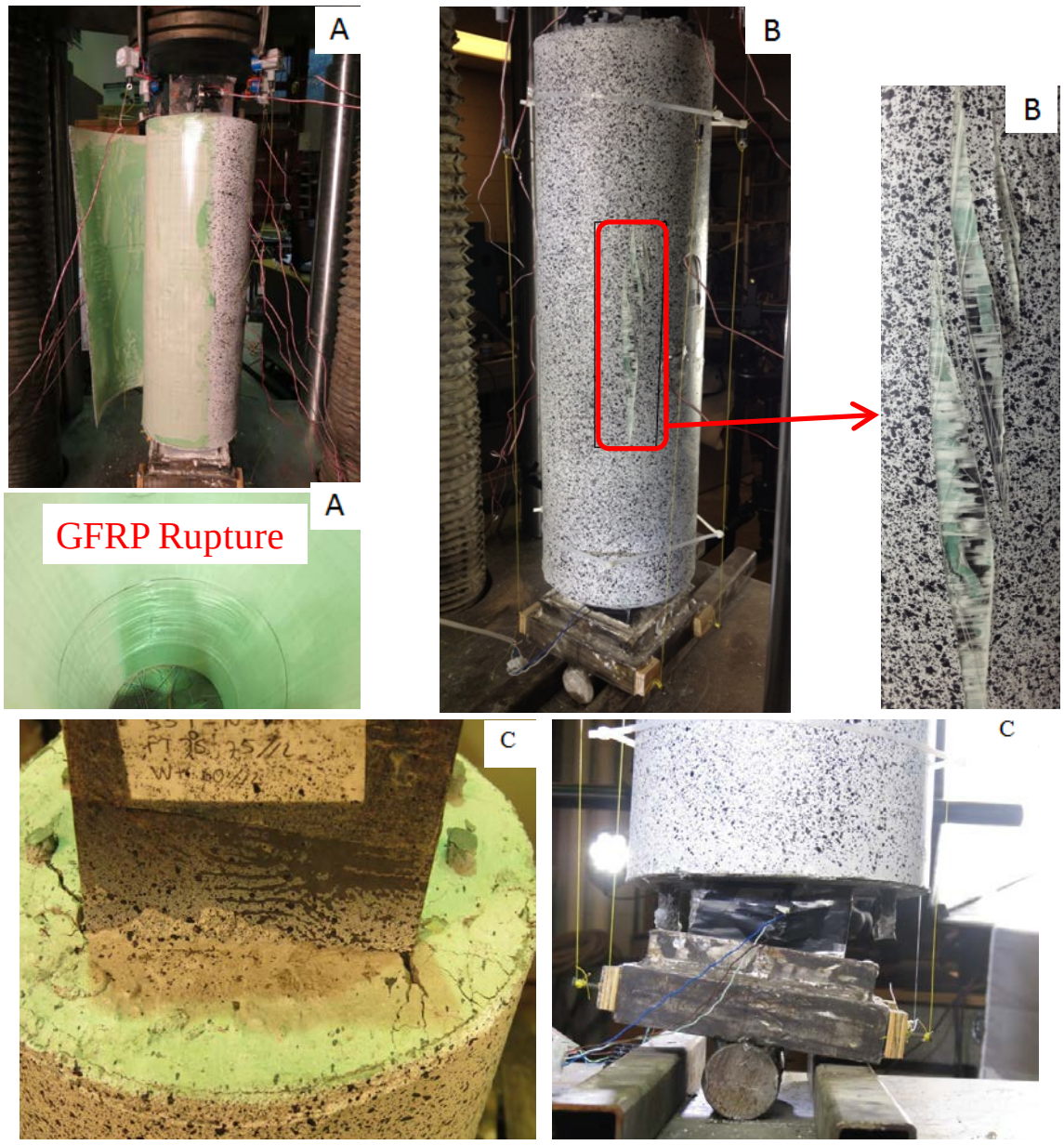

Figure 4.20. A) Failure of G3/2/4#3-2, B) Failure of G3/2/4#4 and C) Failure of G3/3/4#3

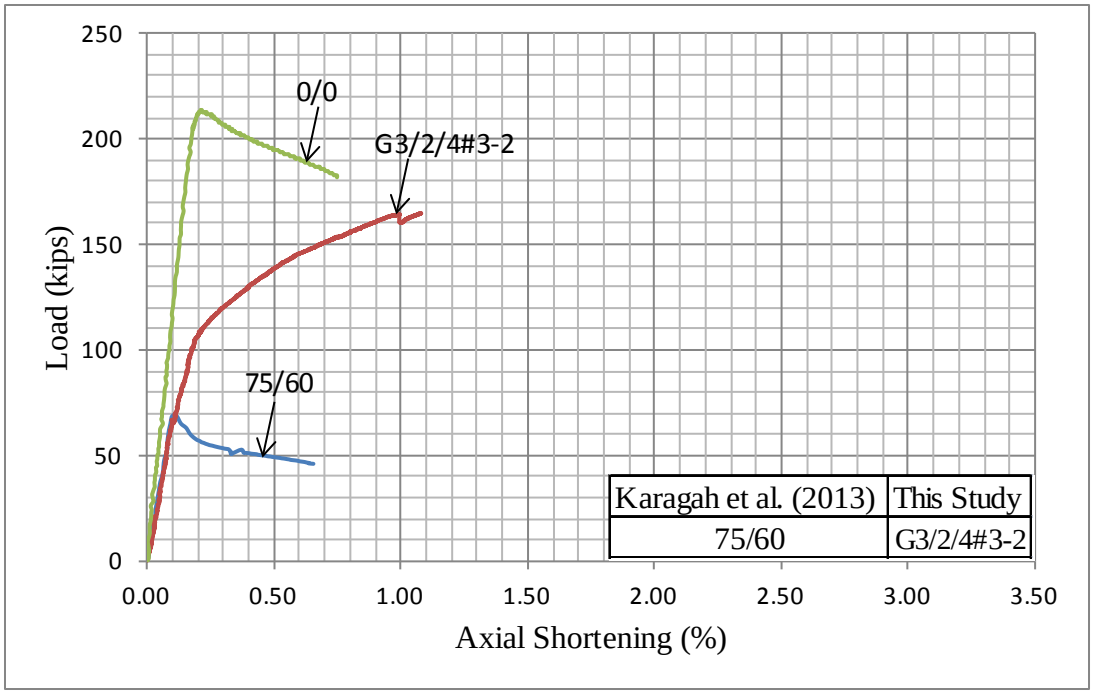

Figure 4.21. Load versus Axial Shortening of G3/2/4#3-2

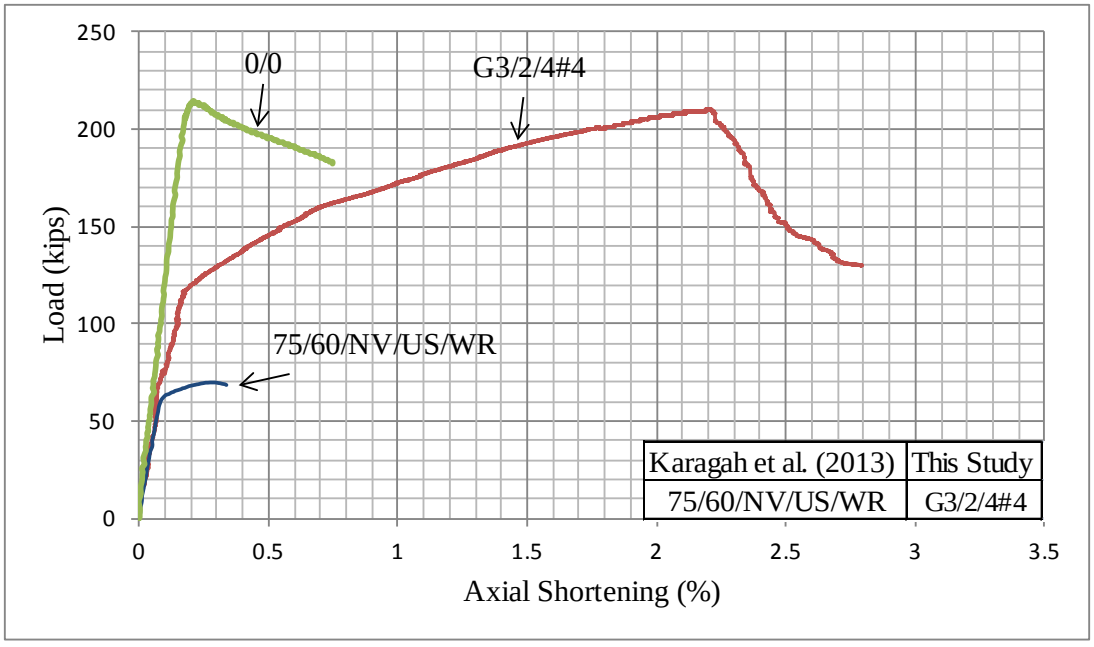

Figure 4.22. Load versus Axial Shortening of G3/2/4#4

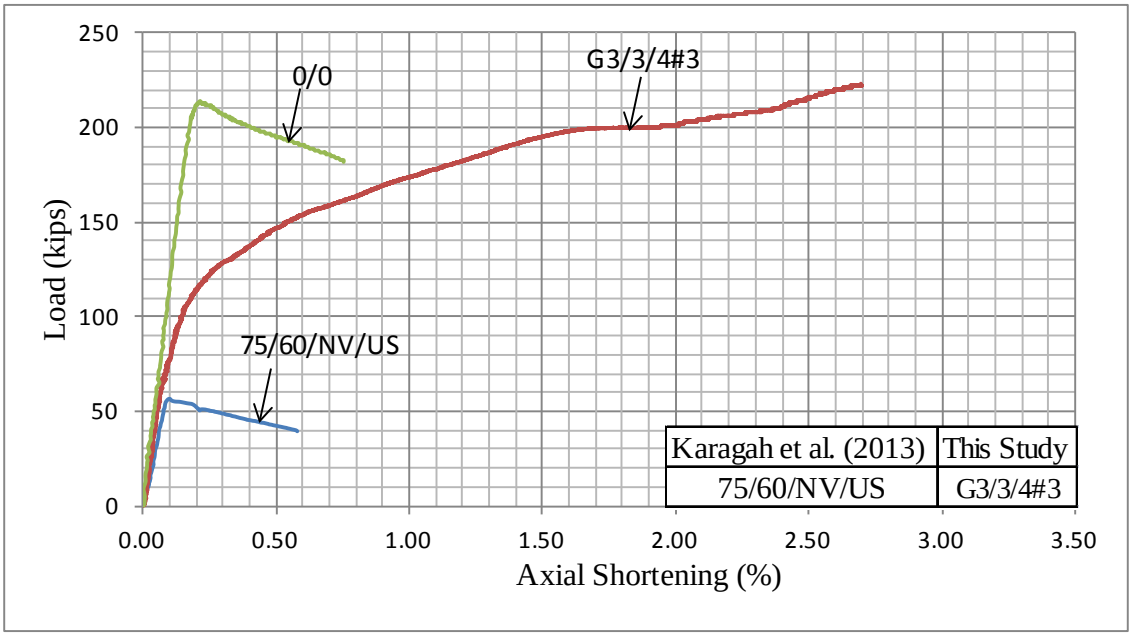

Figure 4.23. Load versus Axial Shortening of G3/3/4#3

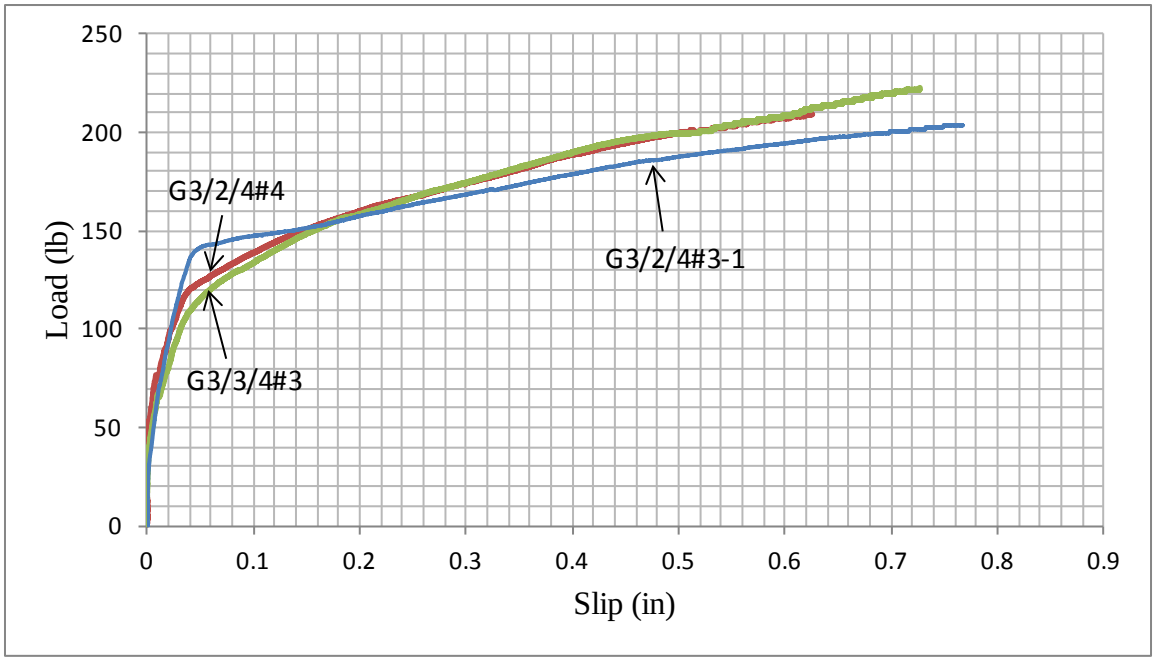

Figure 4.24. Load versus Slip Response of G3/2/4#3-1, G3/2/4#4 and G3/3/4#3

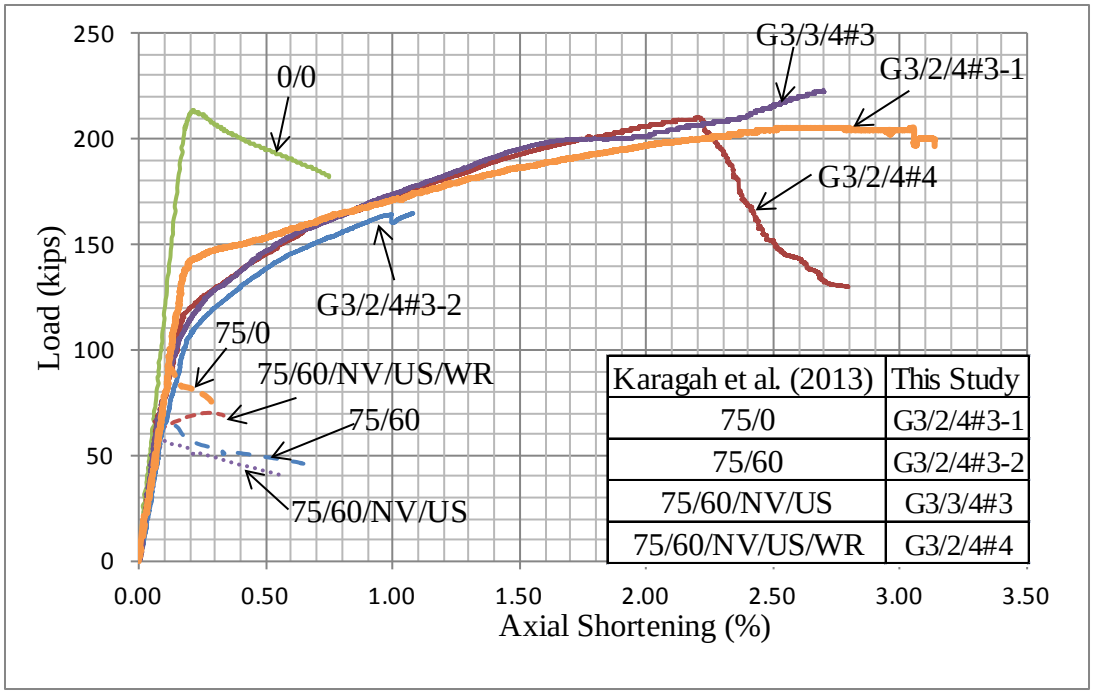

Figure 4.25. Load versus Shortening of Specimens in Group#3

4.4 Behavior of Piles in Group #4

Prior to repair, all the piles in Group #4 failed by flange local buckling at load levels varying from 36 to 40 kips. After reaching their peak loads, loading of the piles continued until the load decreased to levels between 14 and 15 kips. Figure 4.26 presents the axial load-displacement relationships of the damaged piles prior to repair with the GFRP-based system.

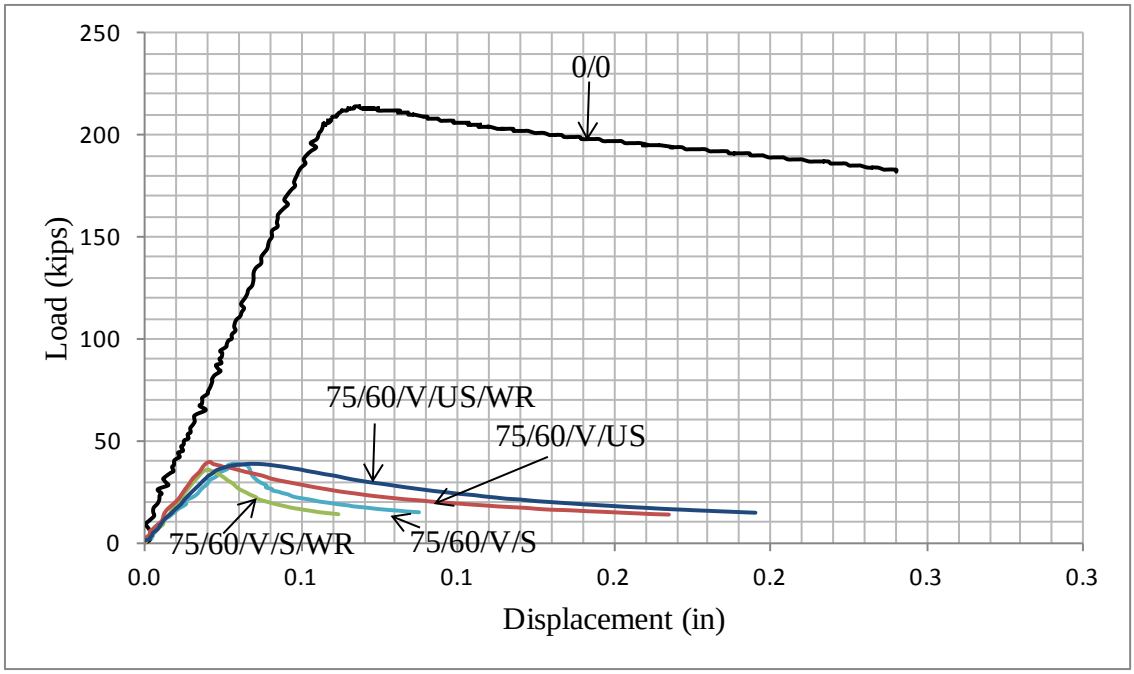

Figure 4.26. The Axial Load-Displacement Relationships of the Damaged Piles in Group #4

Pile G4/2/NR failed at a load level of 149 kips due to GFRP rupture as illustrated in Figure 4.27. Prior to the repair, the pile failed by flange local buckling at a load level of 40 kips. The capacity of the repaired pile was 3.7 times the capacity of the damaged pile and 70% of the capacity of the undamaged control pile. Figure 4.28 compares the axial load-shortening responses of the corroded pile (prior to repair) and the repaired buckled pile (after installation of the jacket) to the response of the undamaged control pile.

Testing of pile G4/2/4#4 demonstrated that the repair system was not correctly installed. Specifically, during casting the concrete began to set prior to completely filling the FRP jacket. Consequently, there were substantial air voids within the jacket. Because of this problem, the increase in capacity of the repaired pile was less than expected. However, the pile did still exhibit a stable hardening post-yield response with large

deformations. Figure 4.29 shows the gap inside of the jacket and the failure mode. This pile failed at a load level of 67 kips. Prior to the repair, the pile failed by flange local buckling at a load level of 36 kips. The capacity of the repaired pile was 1.9 times the capacity of the damaged pile and 31% of the capacity of the undamaged control pile. Figure 4.30 compares the axial load-shortening responses of the corroded pile (prior to repair) and the repaired buckled pile (after installation of the jacket) to the response of the undamaged control pile.

Pile G4/3/NR failed at a load level of 189 kips due to GFRP rupture as illustrated in Figure 4.31. Prior to the repair, the pile failed by flange local buckling at a load level of 40 kips. The capacity of the repaired pile was 4.7 times the capacity of the damaged pile and 88% of the capacity of the undamaged control pile. Figure 4.32 compares the axial load-shortening responses of the corroded pile (prior to repair) and the repaired buckled pile (after installation of the jacket) to the response of the undamaged control pile.

Pile G4/3/4#4 failed at a load level of 212 kips due to buckling of the pile as illustrated in Figure 4.33. Prior to the repair, the pile failed by flange local buckling a load level of 39 kips. The capacity of the repaired pile was 5.4 times the capacity of the damaged pile and 99% of the capacity of the undamaged control pile. Figure 4.34 compares the axial load-shortening responses of the corroded pile (prior to repair) and the repaired buckled pile (after installation of the jacket) to the response of the undamaged control pile. The pile buckled before GFRP ruptured.

The slip between steel pile and concrete for all the specimens in this group is shown in Figure 4.35. In addition, the loads versus axial shortening behavior of all the specimens in Group #4 are compared in Figure 4.36.

Figure 4.27. Failure of G4/2/NR

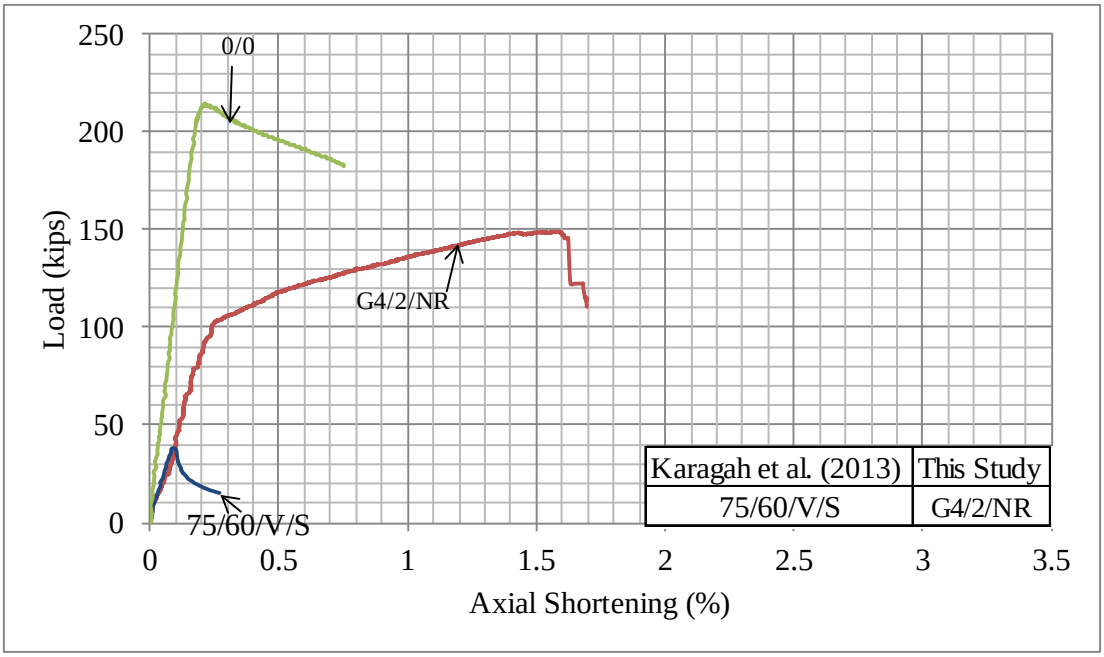

Figure 4.28. Load versus Axial Shortening of G4/2/NR

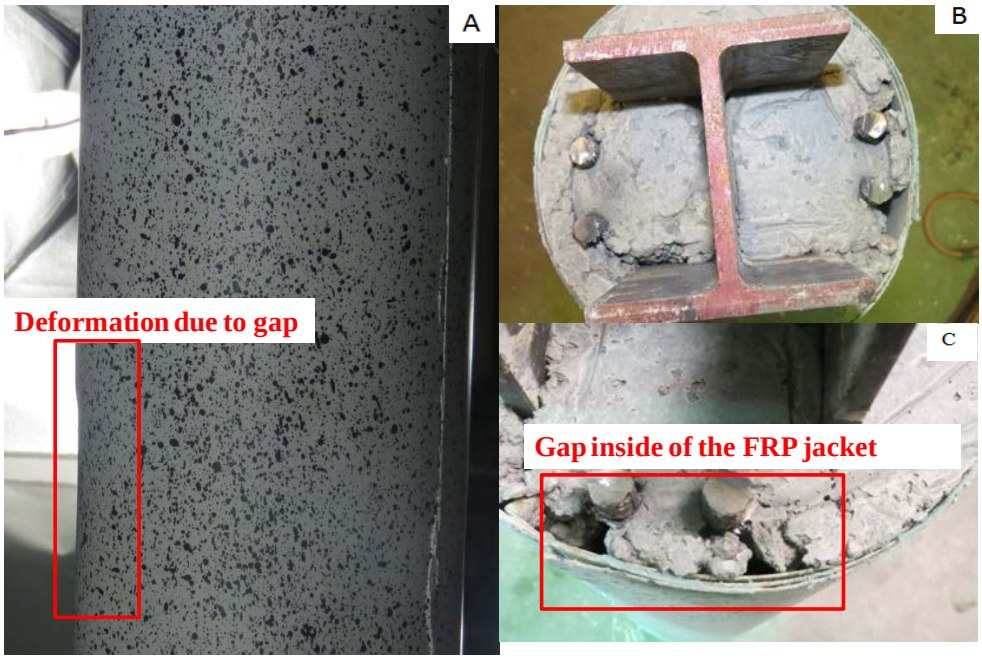

Figure 4.29. A) Failure of Specimen, B and C) Gap for G4/2/4#4

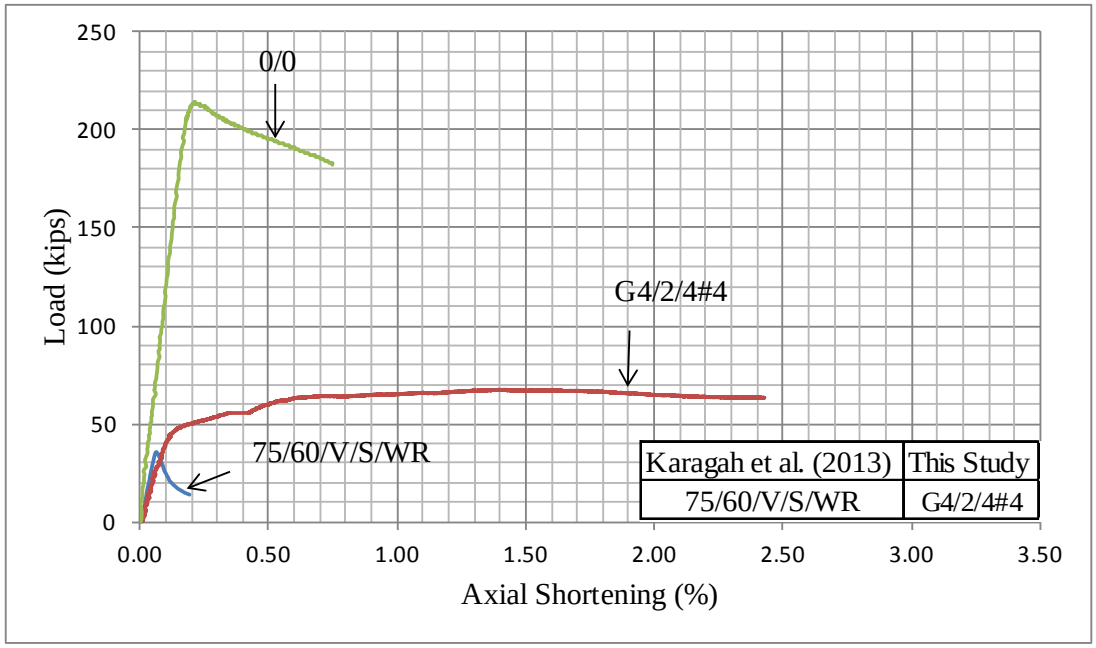

Figure 4.30. Load versus Shortening of G4/2/4#4

Figure 4.31. Failure of G4/3/NR

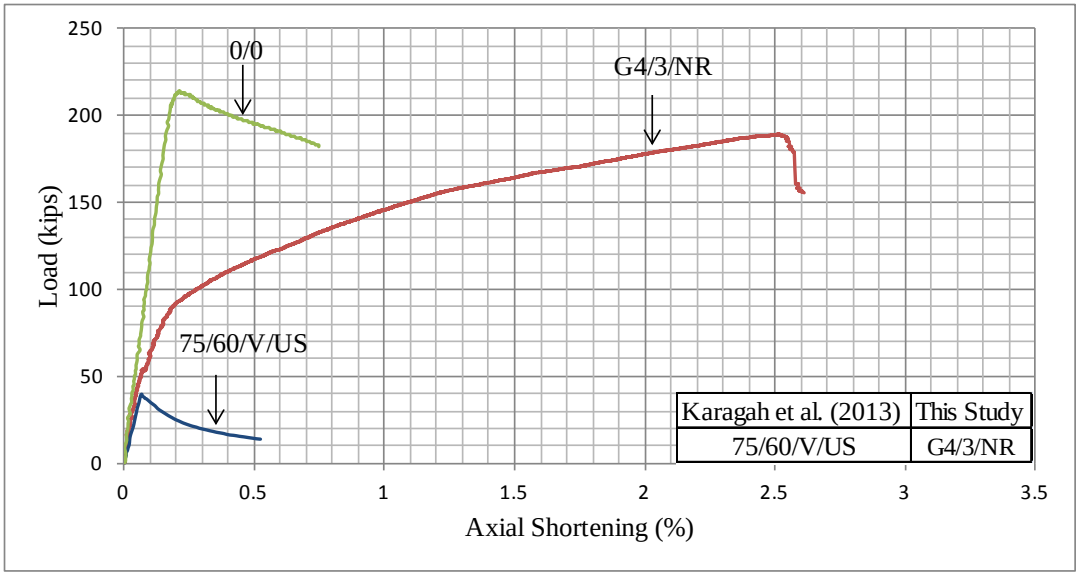

Figure 4.32. Load versus Axial Shortening of G4/3/NR

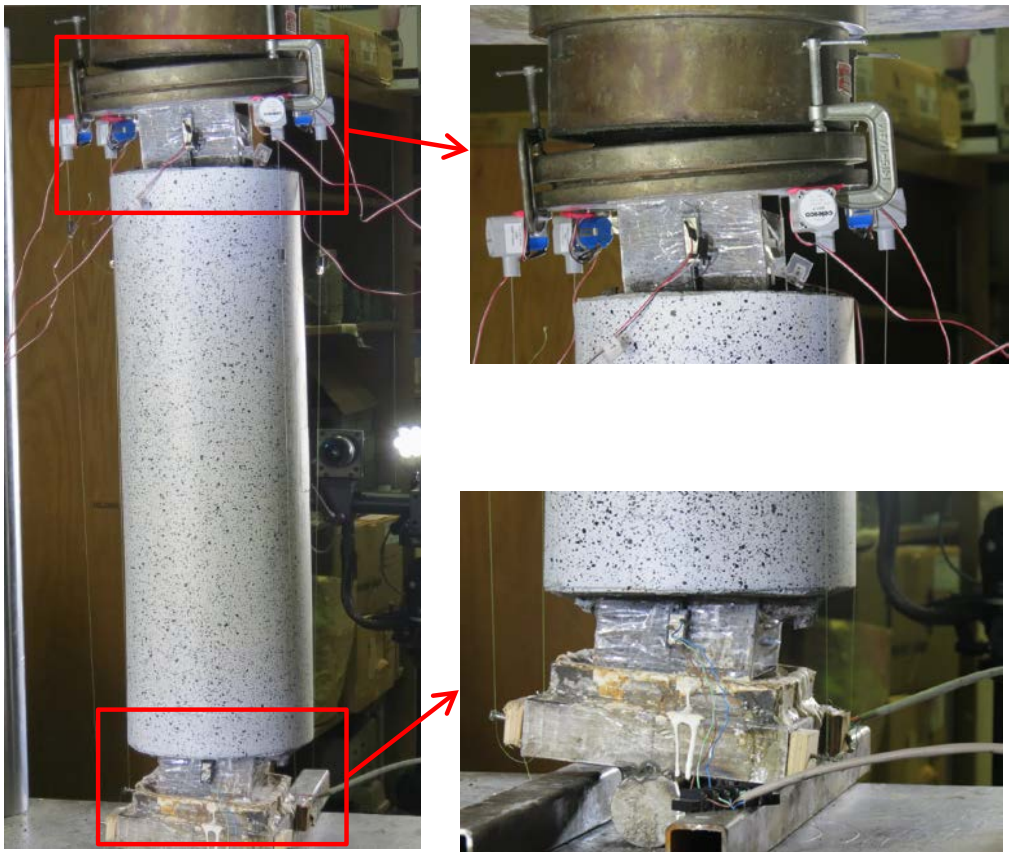

Figure 4.33. Failure of G4/3/4#4

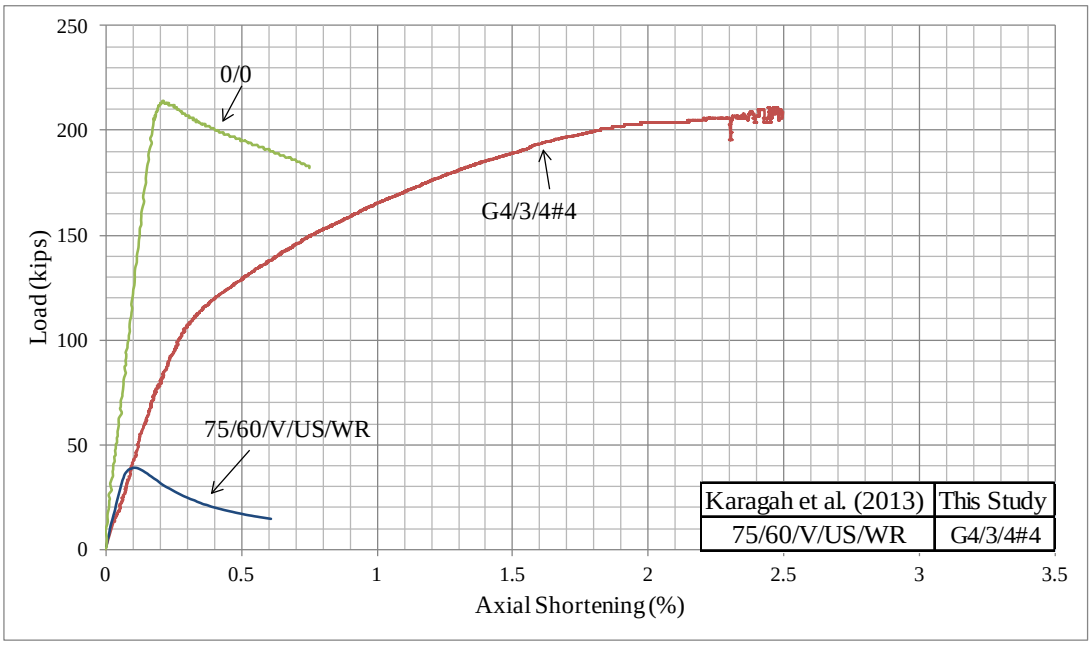

Figure 4.34. Load versus Axial Shortening of G4/3/4#4

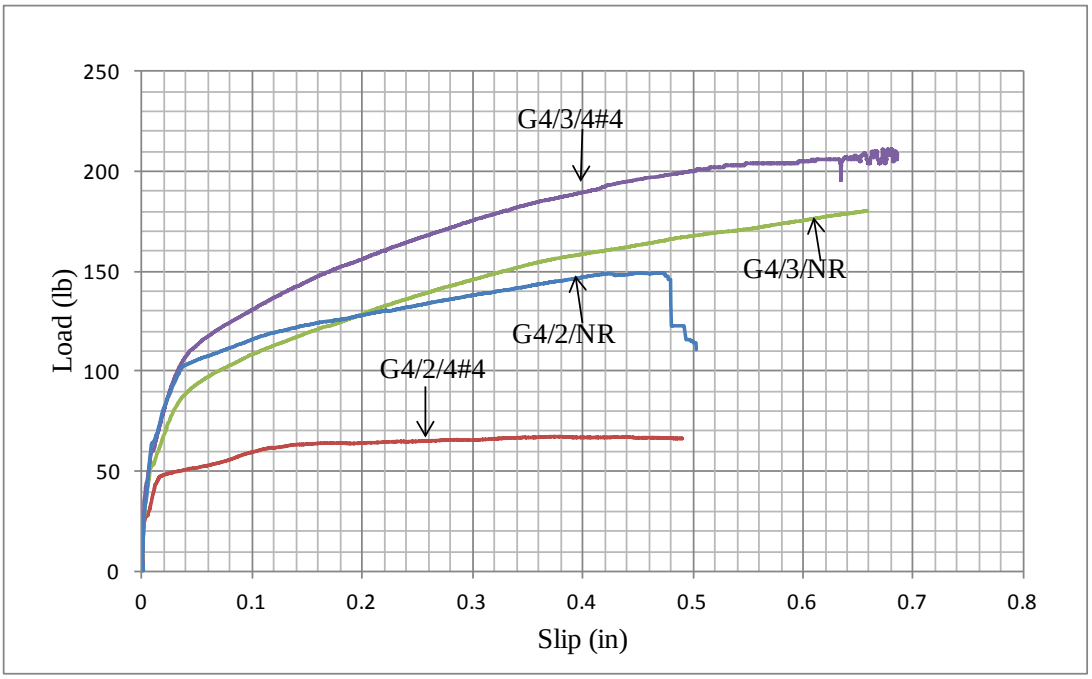

Figure 4.35. Load versus Slip of G4/3/4#4, G4/3/NR, G4/2/NR and G4/2/4#4

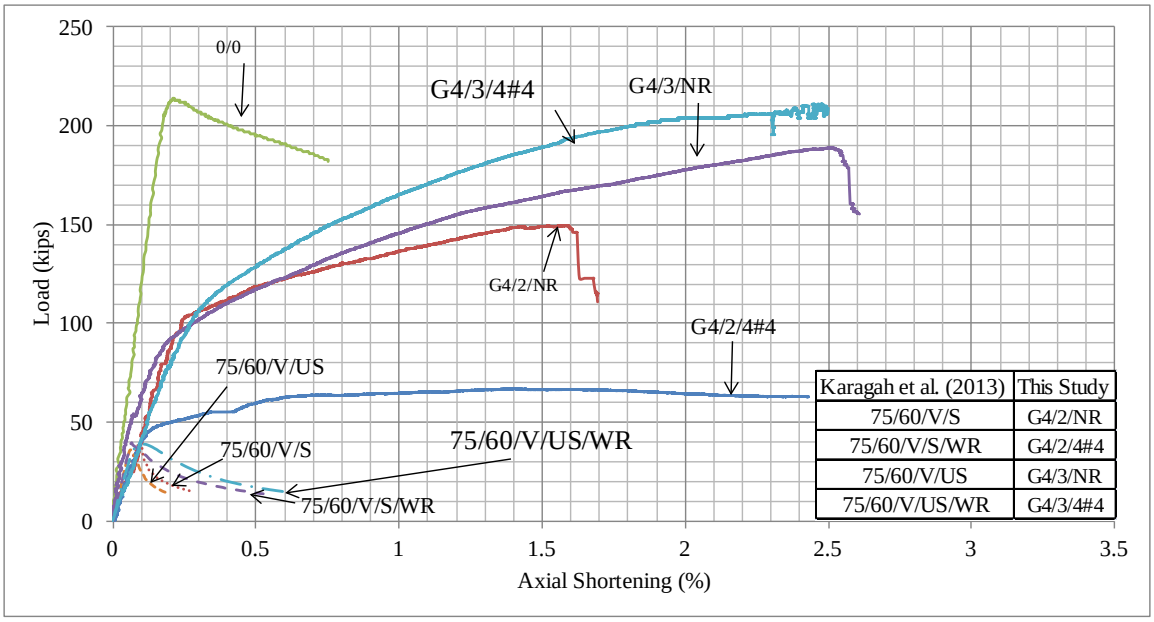

Figure 4.36. Load versus Shortening of Specimens in Group#4

Comparing the response of the damaged piles to the response of the repaired piles highlights a key trend. The damaged piles generally exhibited a descending post-peak behavior after buckling. This could lead to reduced capacity to redistribute load and system instability in a bridge or building after buckling of a few piles. In contrast, the load carrying capacity of the repaired piles continued to increase after the onset of buckling. This hardening behavior is expected to produce a more stable system response and is preferable to minimize the likelihood of progressive collapse. A similar trend was observed for all of the tested piles.

Table 4.2 presents the maximum measured axial load for each of the tested piles before and after repair. The table also gives the elastic axial stiffness of the piles before and after repair. The table also presents the measured lateral deflection at the mid-height of the piles prior to installation of the repair system.

Table 4.2. Test Results

	Designation		Loss of Cross Section (%)	Initial Out of Straightness (in)**	Compressive Strength (kips)			Axial Stiffness (kips/in)		
	Karagah et al. (2013)	This Study			Unrepaired	Repaired	Ratio***	Unrepaired	Repaired	Ratio***
Group #1	0/0	G1/2/NR-1	0	0.59	215	202	0.940	3538.7	1921.5	0.543
	0/30	G1/2/NR-2	9	0.31	201	204	1.015	4178.2	2329.4	0.558
	0/60	G1/2/NR-3	16.06	0.44	178	212	1.191	3552.8	2376.1	0.669
Group #2	50/0	G2/3/NR-1	39.9	0.44	117	216	1.846	3740.2	1841.1	0.492
	50/30	G2/3/NR-2*	43.55	0.88	130	196.5	1.512	3614.7	1347.3	0.373
Group #3	75/0	G3/2/4#3-1	58.88	0.25	92	205	2.228	2406.3	2454.4	1.020
	75/60	G3/2/4#3-2	67.64	0.16	70	164.4	2.349	2091.8	2109.7	1.009
	75/60/NV/US	G3/3/4#3	75.43	0.44	57	223	3.912	2053.6	2329.8	1.134
	75/60/NV/US/WR	G3/2/4#4	74.7	0.10	70	210	3.000	2341.6	2024.7	0.865
Group #4	75/60/V/S	G4/2/NR	78.83	0.16	39	149.2	3.826	1372.9	1345.5	0.980
	75/60/V/S/WR	G4/2/4#4	88.32	0.13	36	67	1.861	1939.7	1326.8	0.684
	75/60/V/US	G4/3/NR	78.83	0.25	40	188.9	4.723	1932	1523	0.788
	75/60/V/US/WR	G4/3/4#4	77.37	0.50	39	212	5.436	1634.2	1187.6	0.727

* Total length= 27 inches; repaired length= 20.5 inches

** Initial Imperfection

*** Repaired/Unrepaired

5 Conclusions and Recommendations for Future Research

Thirteen buckled short steel piles with simulated corrosion damage were repaired using concrete-filled glass fiber-reinforced polymer (GFRP) tubes. The piles were subsequently tested under monotonic compression to evaluate the effectiveness of the repair system for rapid emergency repair of buckled steel piles and bridge piles with different levels of corrosion. The effect of different parameters on the response of the repaired piles, including the number of GFRP and the presence and diameter of internal longitudinal steel reinforcing bars were studied. The load carrying capacity and the axial load-shortening response of the repaired piles were compared to those of the corroded ones (prior to repair) and an uncorroded control pile. The research findings led to the following conclusions:

1) The axial capacity of the repaired piles varied from 90 to 444% of the capacity of the undamaged control pile.
2) All of the repaired piles exhibited a hardening response in the non-linear range with increasing load after the onset of non-linearity while the corroded but unrepaired piles typically exhibited a softening response with a decreasing post peak load. The hardening response is preferable to facilitate load redistribution and overall system stability.
3) It was observed that the initial out of straightness affects the stiffness and axial capacity of the piles. Due to initial out of straightness, the repaired piles deflected more than the unrepaired ones during testing.
4) Increasing the number of GFRP layers increased the axial load capacity of composite piles. When similar specimens were compared, with two and three layers of GFRP

the axial load capacity increased by more than 80%. This was attributed to the increase of the confining pressure that was provided by the thicker GFRP jacket.

5) The observed failure modes for these piles were the debonding and rupture of the GFRP. One of the specimens failed by debonding due to improper sanding of the laminate. For the other specimens, this failure mode was not dominant after improvement of the sanding procedure.
6) Increasing the diameter of the internal longitudinal steel reinforcing bars from #3 to #4, repairs increased the capacity of similar piles by 65%. The size of rebar did not significantly affect the axial stiffness of the composite piles.

The findings indicate a need for future research in the following areas:

1) The current study focused on small-scale short steel piles. Validation of the results based on large-scale or full-scale testing is recommended.
2) The effect of replacing the GFRP jackets with stiffer CFRP jackets should also be investigated. Additionally, the influence of using other types of grouting materials such as rapid curing cementitious materials (magnesium phosphate and aluminum phosphate cements) should be considered as a method to shorten the time needed to conduct the repairs.
3) The effectiveness of the repair system on piles with different slenderness and cross-sectional geometries should be investigated.
4) The effectiveness of the repair technique for repair of piles subjected to axial loads and bending moments should be evaluated.

5) A numerical model should be developed to predict the response of the repaired piles. The development of a numerical model would facilitate the development of design-oriented models.
6) The bond behavior between the components of the repair system (concrete- steel and concrete-fiber-reinforced polymer bonds) should be thoroughly investigated and the effect of the bond on the overall response of the repaired piles should be quantified.
7) Different repair lengths should be evaluated as this parameter relates to the cost and performance.
8) The long-term durability of the repair technique should be investigated.

REFERENCES

AASHTO LRFD Bridge, Design Specifications. American Association of State Highway and Transportation officials (AASHTO), 2012.

ASTM International. (2012). "A370-12a Standard Test Methods and Definitions for Mechanical Testing of Steel Products." West Conshohocken, PA.

ASTM International. (2008). "D3039M-08 Standard Test Methods for Tensile Properties of Polymer Matrix Composite Materials." West Conshohocken, PA.

ASTM International. (2010). "D7565M-10 Standard Test Methods for Determining Tensile Properties of Fiber Reinforced Polymer Matrix Composites Used for Strengthening of Civil Structures." West Conshohocken, PA.

ASTM International. (2003). "C39M-03 Standard Test Method for Compressive Strength of Cylindrical Concrete Specimens." West Conshohocken, PA.

El- Tawil, S. and Ekiz, E., (2009). "Inhibiting Steel Brace Buckling Using Carbon Fiber-Reinforced Polymers: Large-Scale Test." *Journal of Structural Engineering* ASCE/ May 2009.

Feng, P., Zhang, Y., Bai, Y., and Ye, L. (2013). "Strengthening of Steel Members in Compression by Mortar Filled FRP Tubes" *Thin-Walled Structures* 64 (2013) 1-12.

Han, L., Tao, Z., Liao, F., and Xu, Y., (2010). "Tests on Cyclic Performance of FRP-Concrete-Steel Double-Skin Tubular Columns." *Thin- walled Structure* 48 (2010) 430-439.

Harries, K. A., and Carey, S. A. (2002). "Shape and "Gap" Effects on the Behavior of Variably Confined Concrete" *Cement and Concrete Research* 33 (2003) 881–890.

Karagah, H., and Dawood, M. (2013). "Axial Capacity of Partially Corroded Steel Bridge Pilese." *Proceedings of the Annual Stability Conference Structural Stability Research Council,* St. Louis, Missouri, April16-20, 2013.

Karimi, K., Tait, M. J., and El-Dakhakhni, W. W. (2010). "Testing and Modeling of a Novel FRP-Encased Steel-Concrete Composite Column" *Composite Structures* 93 (2011) 1463-1473.

Karimi, K., El-Dakhakhni, W. W., and Tait, M. J. (2012). "Behavior of Slender Steel-Concrete Composite Columns Wrapped with FRP Jackets" *Journal of Performance of Constructed Facilities,* Vol. 26, No.5, October 1, 2012, ASCE.

Lam, L., and Teng, J. G. (2003). "Design-Oriented Stress-Strain Models for FRP-Confined Concrete" *J. Const. Build. Mat.*, 17(6-7), 471-489.

Liu, X., Nanni, A., and Silva, P. F. (2005). "Rehabilitation of Compression Steel Members Using FRP Pipes Filled with Non-Expansive and Expansive Light-weight Concrete" *Advences in Structural Engineering* Vol. 8 No.2 2005.

Shi, C., Karagah, H., Dawood, M., and Belarbi, A., (2014). "Numerical Investigation of H-Shaped Short Steel Piles With Localized Severe Corrosion." *Engineering Structures* 73 (2014) 114-124.

Appendix A: Strain Gages Data

Specimens G3/2/4#3-2, G3/2/4#4, G3/3/4#3, G3/2/4#3-1, G1/2/NR-3 and G4/2/NR were instrumented with strain gages. Specimens G1/2/NR-1, G1/2/NR-2, G2/3/NR-1, G2/3/NR-2, G4/2/4#4, G4/3/NR and G4/3/4#4 were not instrumented with strain gages.

Specimen G3/2/4#3-2

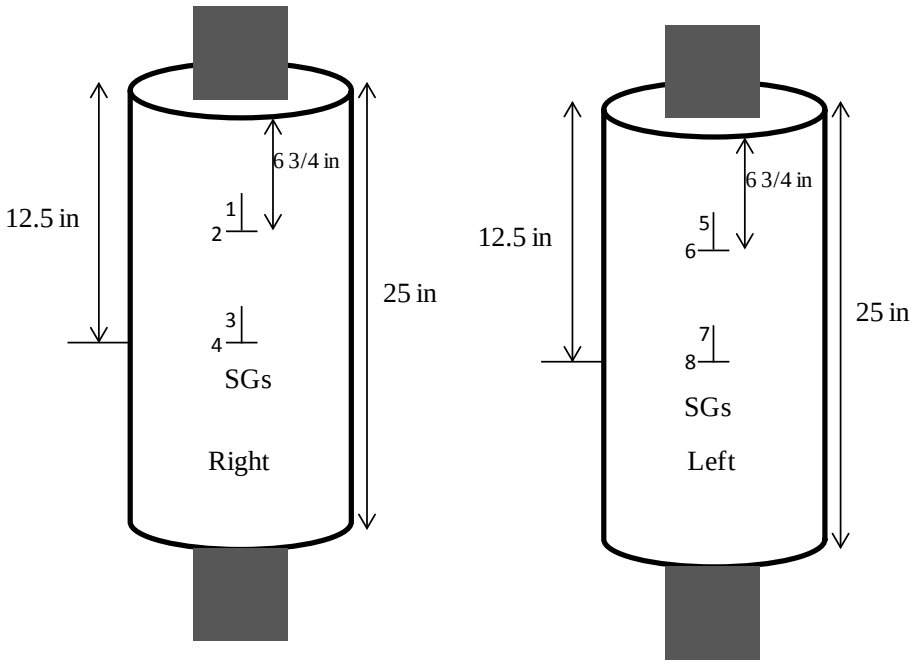

Figure A.1. Locations of Strain Gages for Specimen G3/2/4#3-2

Designation		Loss of Cross Section (%)	Initial Out of Straightness (in)	Compressive Strength (kips)			Axial Stiffness (kips/in)		
Karagah et al. (2013)	This Study			Unrepaired	Repaired	Ratio	Unrepaired	Repaired	Ratio
75/60	G3/2/4#3-2	67.64	0.16	70	164.4	2.349	2091.8	2109.7	1.009

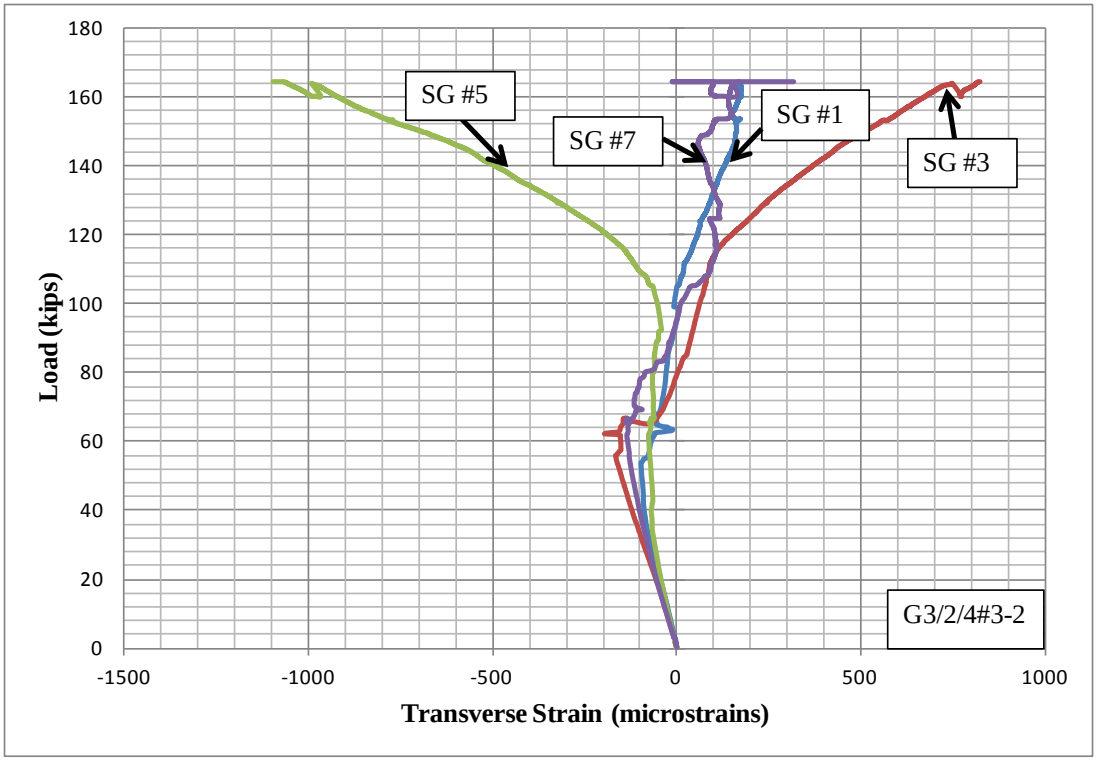
SG #5
SG #7
SG #1
SG #3
G3/2/4#3-2
Load (kips)
Transverse Strain (microstrains)
180
160
140
120
100
80
60
40
20
0
-1500
-1000
-500
0
500
1000

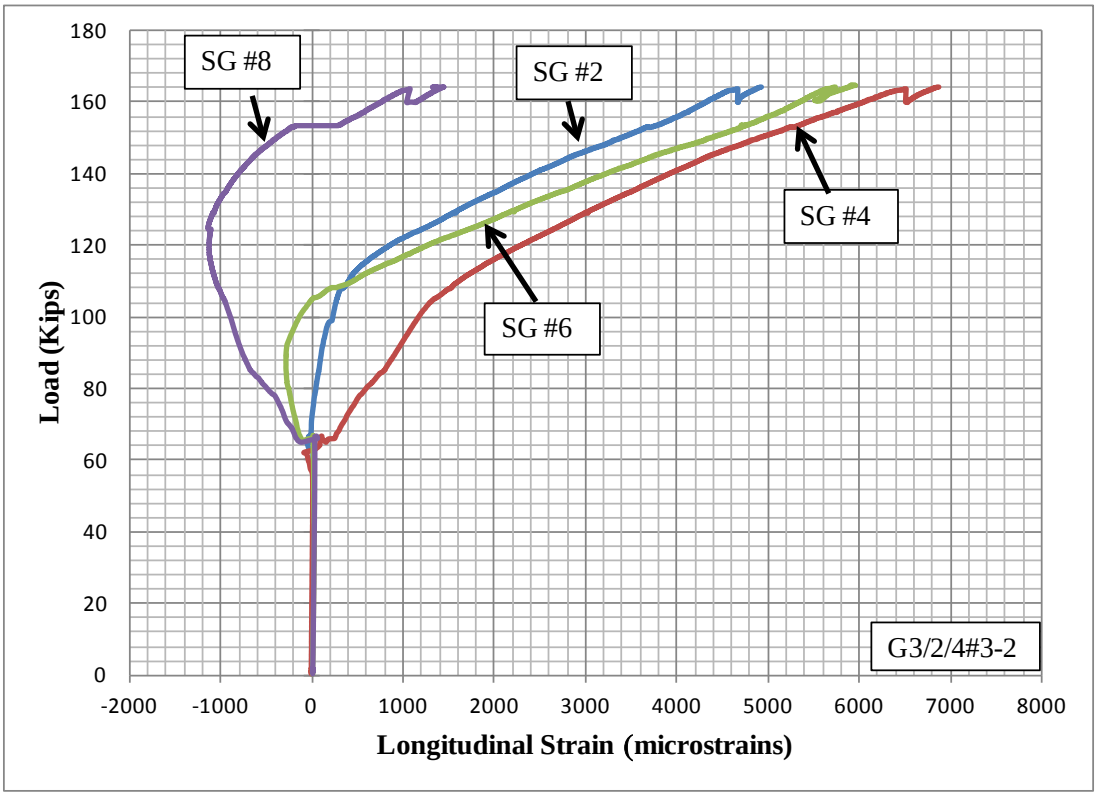
SG #8
SG #2
SG #4
SG #6
G3/2/4#3-2
Load (Kips)
Longitudinal Strain (microstrains)
180
160
140
120
100
80
60
40
20
0
-2000
-1000
0
1000
2000
3000
4000
5000
6000
7000
8000

Specimens G3/2/4#4

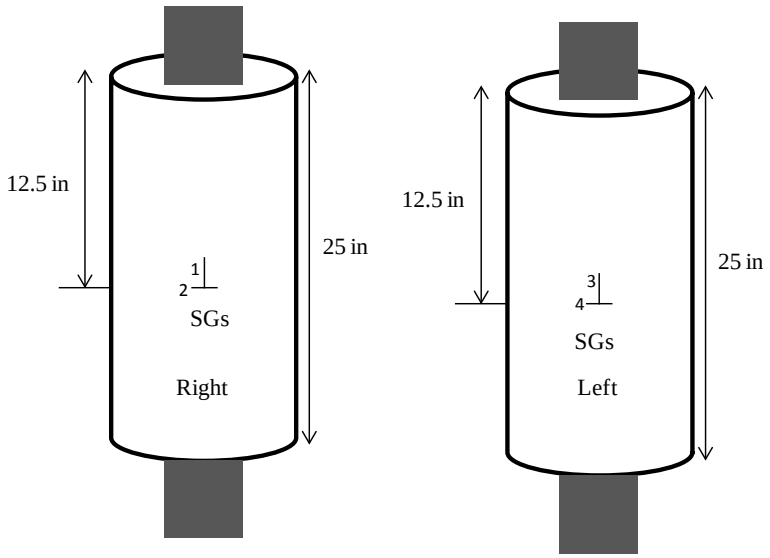

Figure A.2. Locations of Strain Gages for Specimens G3/2/4#4

Designation		Loss of Cross Section (%)	Initial Out of Straightness (in)	Compressive Strength (kips)			Axial Stiffness (kips/in)		
Karagah et al. (2013)	This Study			Unrepaired	Repaired	Ratio	Unrepaired	Repaired	Ratio
75/60/NV/US/WR	G3/2/4#4	74.7	0.10	70	210	3.000	2341.6	2024.7	0.865

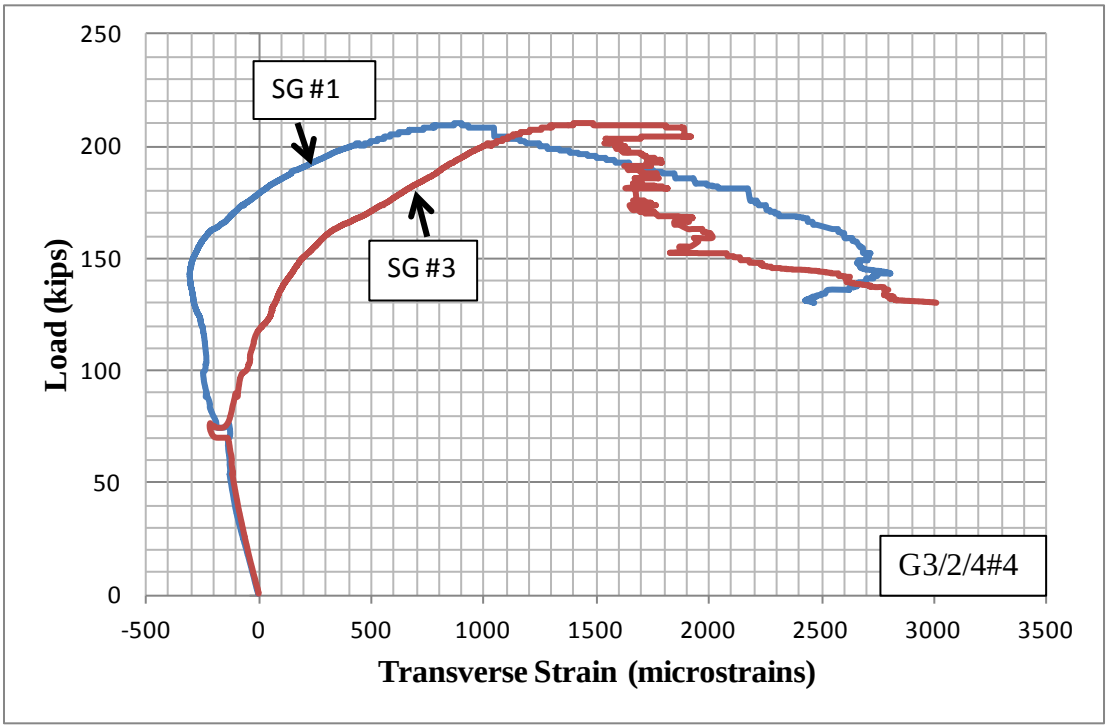

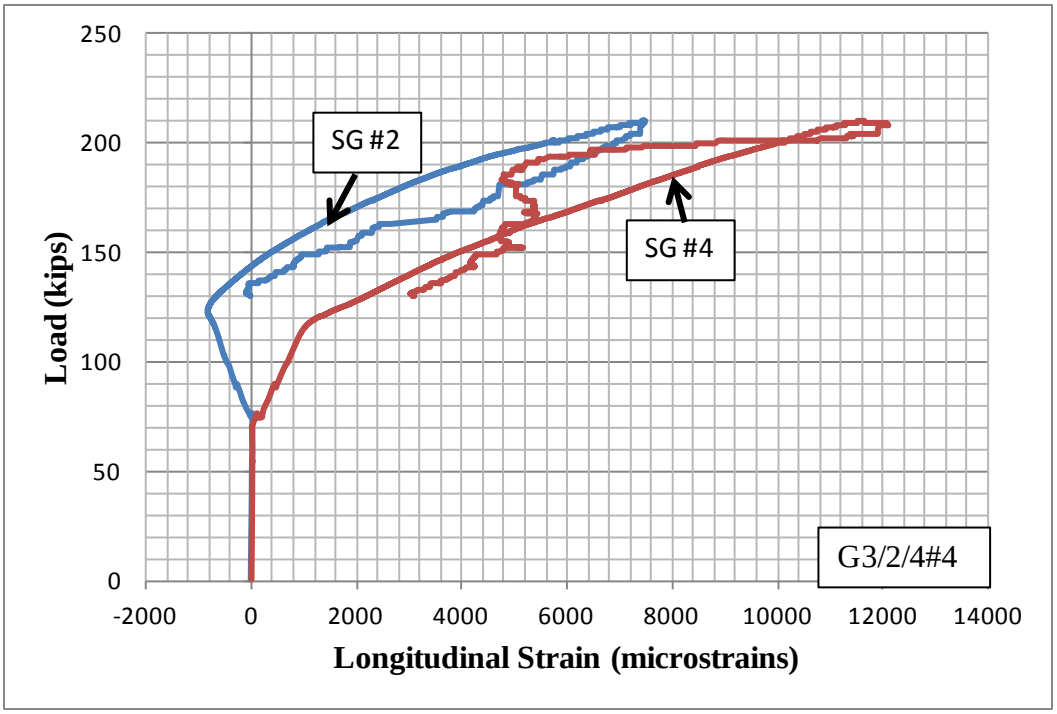

Specimens G3/3/4#3

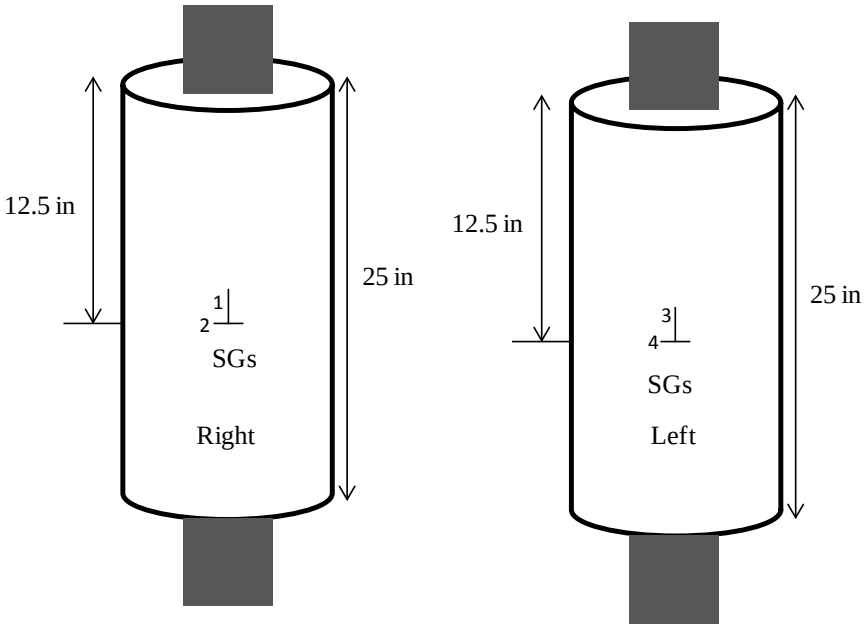

Figure A.3. Locations of Strain Gages for Specimen G3/3/4#3

Designation		Loss of Cross Section (%)	Initial Out of Straightness (in)	Compressive Strength (kips)			Axial Stiffness (kips/in)		
Karagah et al. (2013)	This Study			Unrepaired	Repaired	Ratio	Unrepaired	Repaired	Ratio
75/60/NV/US	G3/3/4#3	75.43	0.44	57	223	3.912	2053.6	2329.8	1.134

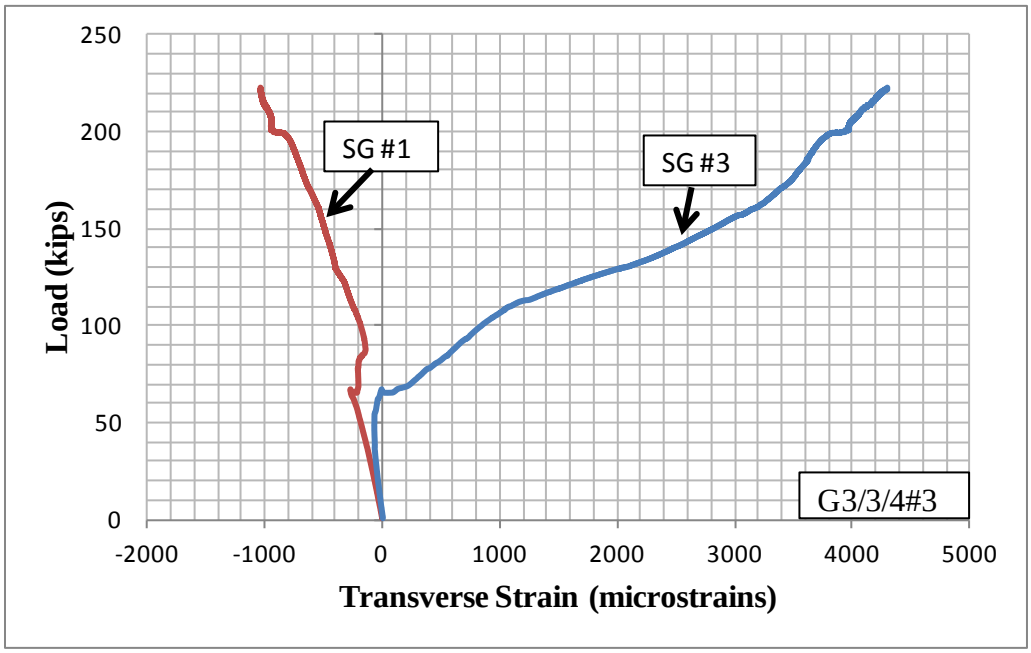

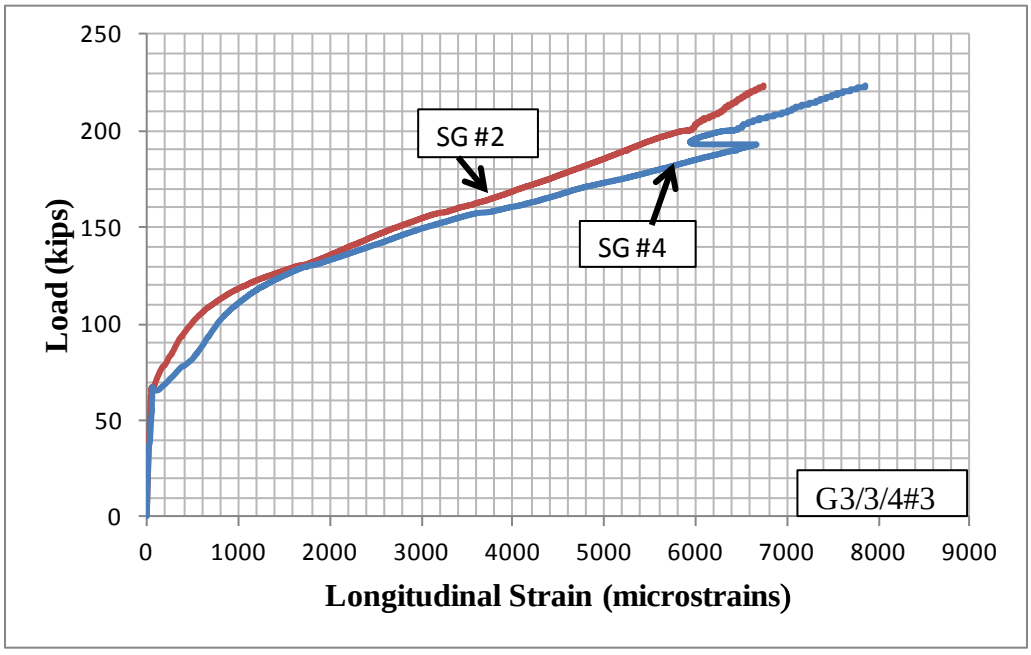

Specimens G3/2/4#3-1

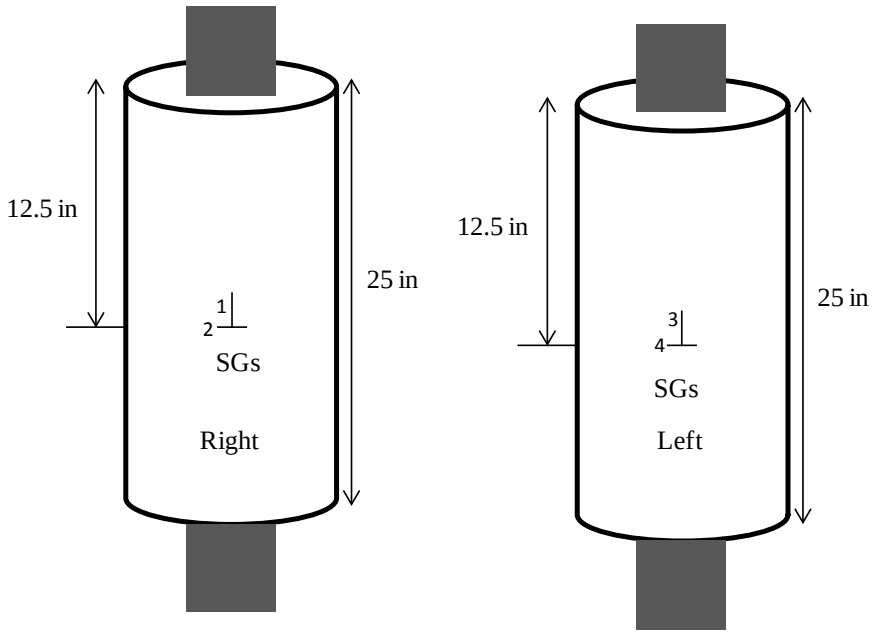

Figure A.4. Locations of Strain Gages for Specimens G3/2/4#3-1

Designation		Loss of Cross Section (%)	Initial Out of Straightness (in)	Compressive Strength (kips)			Axial Stiffness (kips/in)		
Karagah et al. (2013)	This Study			Unrepaired	Repaired	Ratio	Unrepaired	Repaired	Ratio
75/0	G3/2/4#3-1	58.88	0.25	92	205	2.228	2406.3	2454.4	1.020

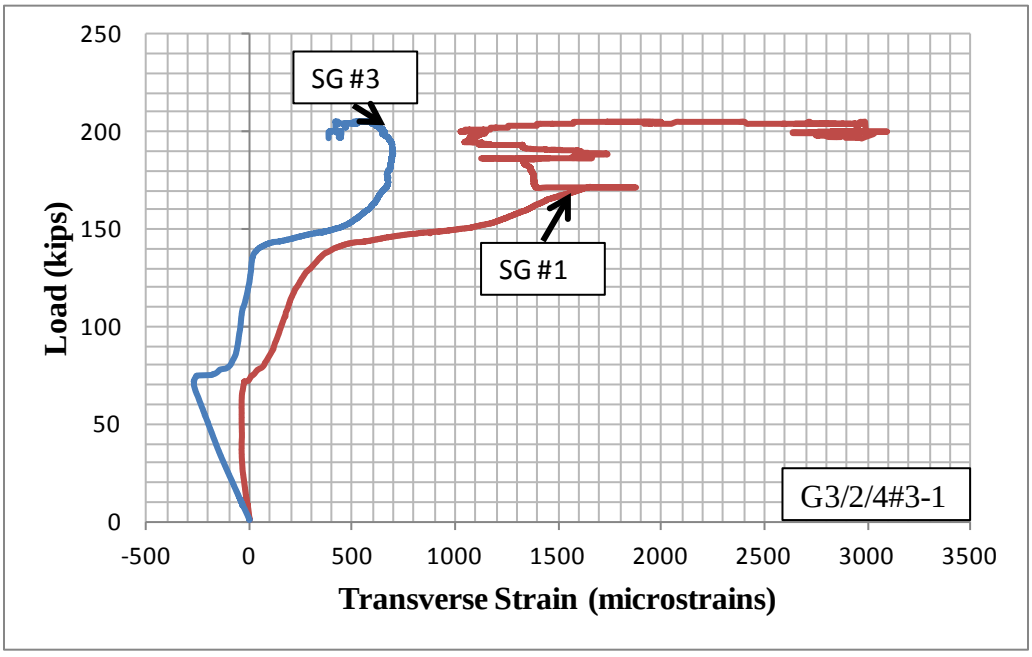

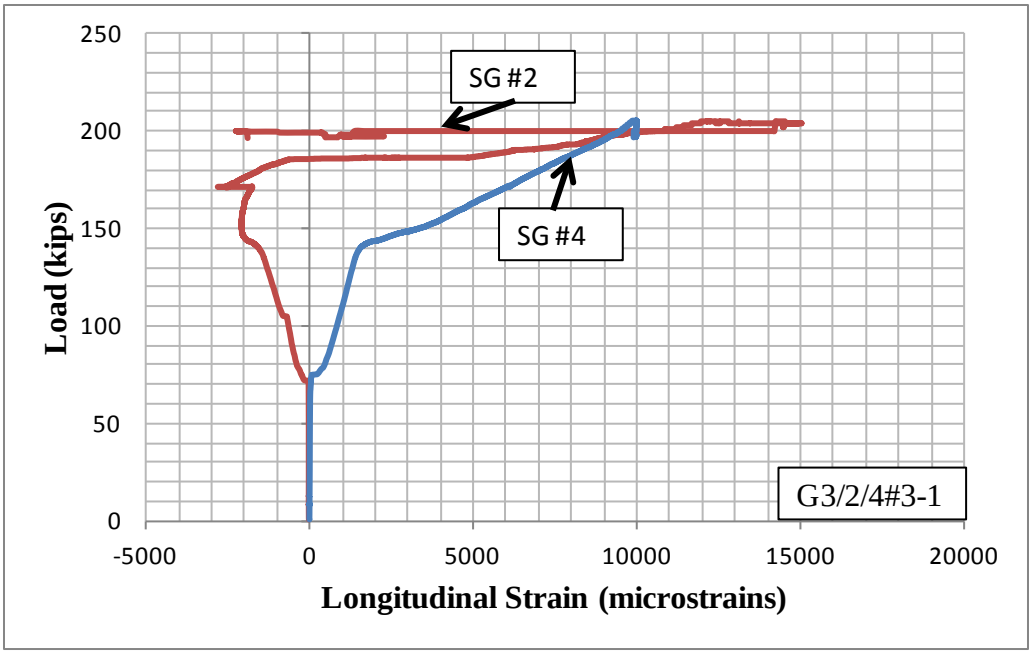

Specimens G1/2/NR-3

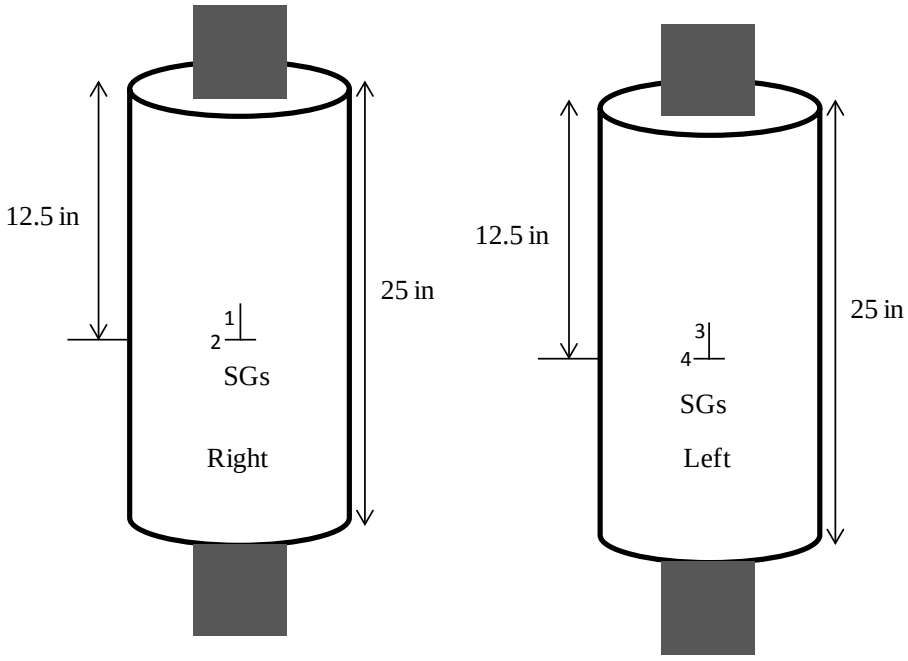

Figure A.5. Locations of Strain Gages for Specimens G1/2/NR-3

Designation		Loss of Cross Section (%)	Initial Out of Straightness (in)	Compressive Strength (kips)			Axial Stiffness (kips/in)		
Karagah et al. (2013)	This Study			Unrepaired	Repaired	Ratio	Unrepaired	Repaired	Ratio
0/60	G1/2/NR-3	16.06	0.44	178	212	1.191	3552.8	2376.1	0.669

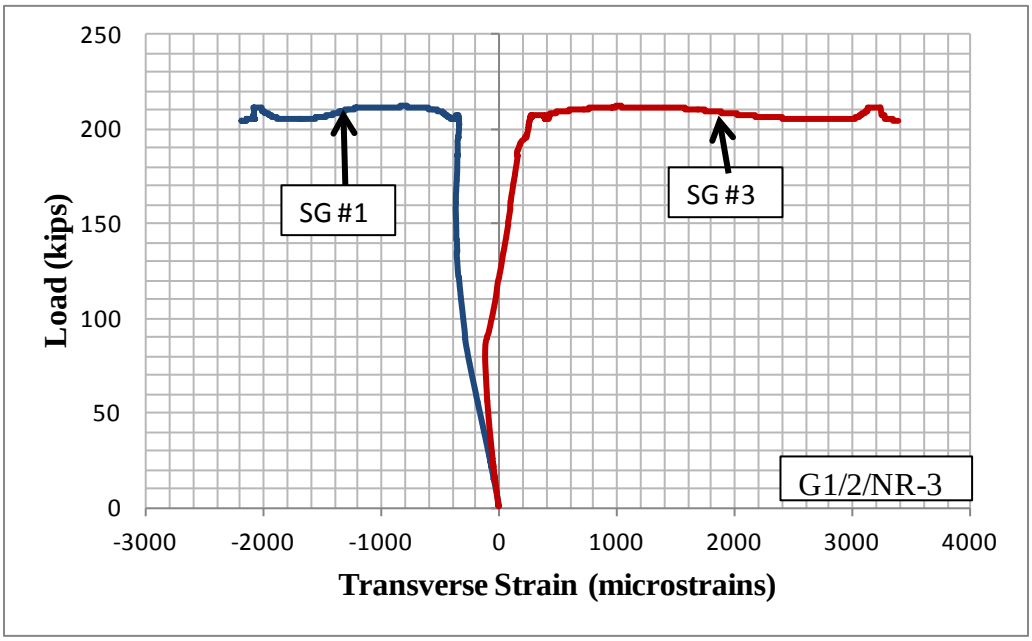

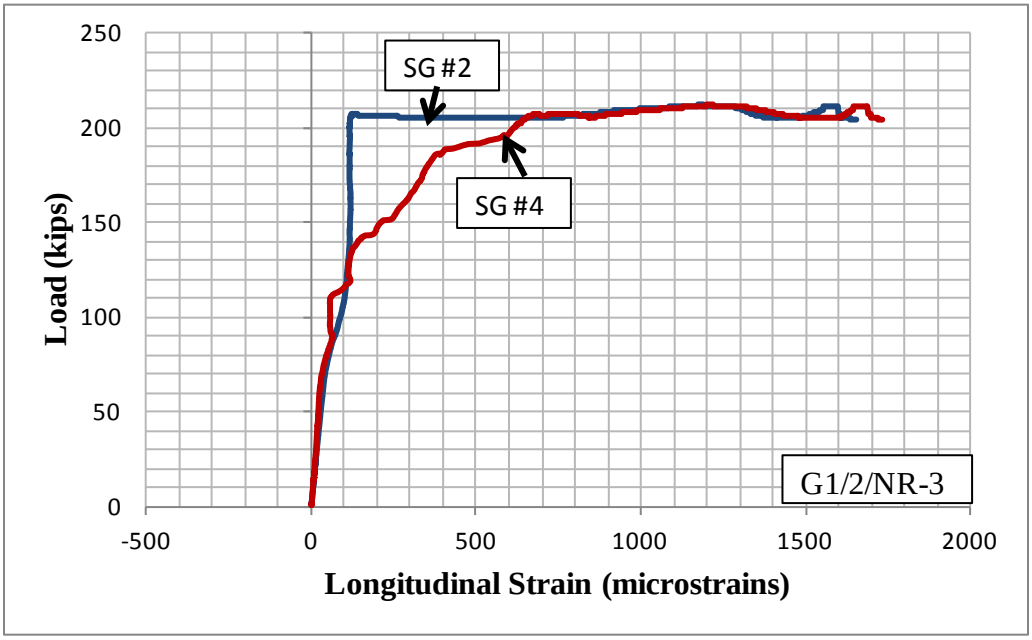

Specimens G4/2/NR

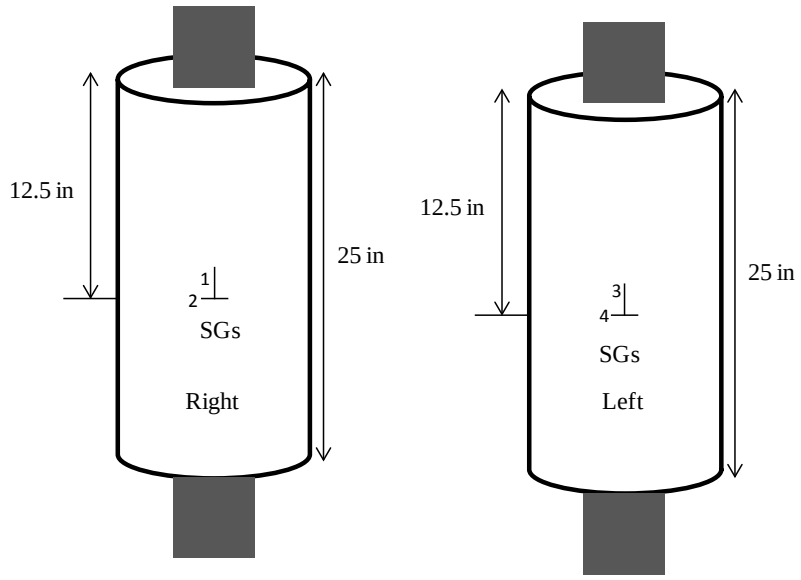

Figure A.6. Locations of Strain Gages for Specimens G4/2/NR

Designation		Loss of Cross Section (%)	Initial Out of Straightness (in)	Compressive Strength (kips)			Axial Stiffness (kips/in)		
Karagah et al. (2013)	This Study			Unrepaired	Repaired	Ratio	Unrepaired	Repaired	Ratio
75/60/V/S	G4/2/NR	78.83	0.16	39	149.2	3.826	1372.9	1345.5	0.980

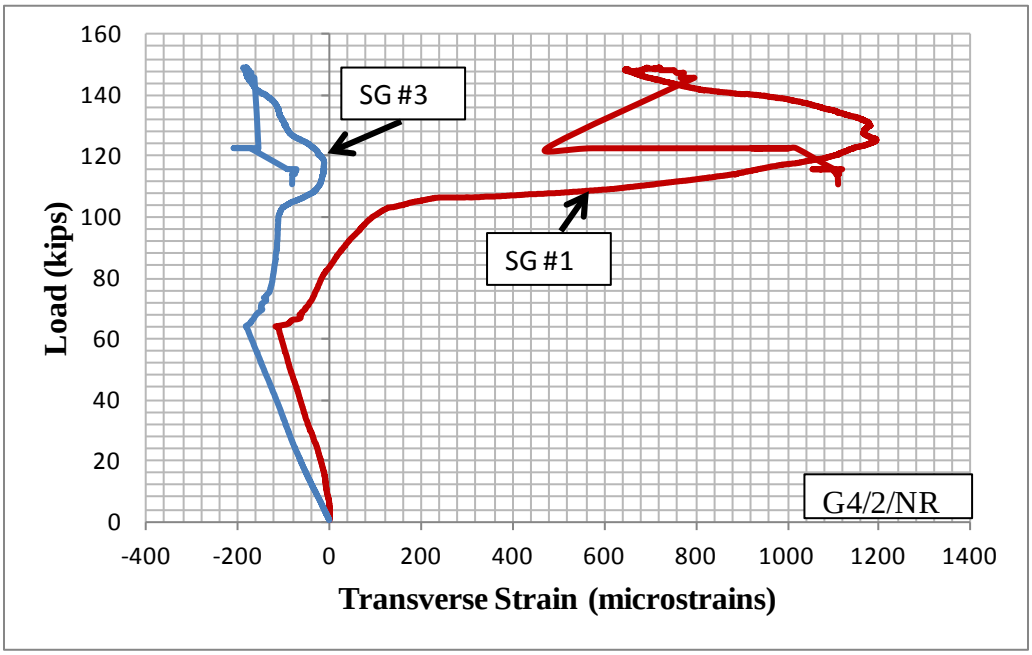

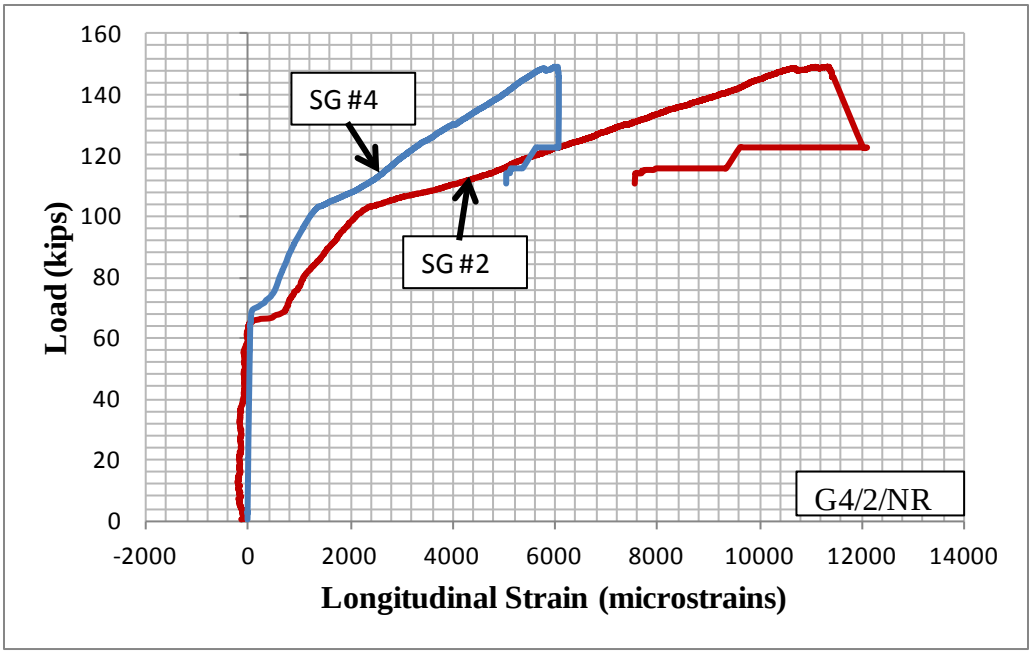
160
140
120
100
80
60
40
20
0
Load (kips)
SG #4
SG #2
G4/2/NR
-2000
0
2000
4000
6000
8000
10000
12000
14000
Longitudinal Strain (microstrains)